LBL--30866

DE93 001545

Energy Conversion & Storage Program 1990 Annual Report

Elton J. Cairns, *Program Leader*

Applied Science Division
Lawrence Berkeley Laboratory
University of California
Berkeley, California 94720
(510) 486-5001

LBL-30866

Energy Conversion & Storage Program Staff

Elton J. Cairns, ***Program Leader***

Thomas Adler
Eduardo Baralt
Ali Barootkoop
Nicolas Barthelemy
Paul Berdahl
William Berry
Rosemary Bittmann
Harvey Blanch
Nerilso Bocchi
Gessie Brissard
Robert Broekhuis
Garth Burns
Karen Bustillo
Wanqing Cao
Van Carey
Wing-Tat Chan
Ernest Chen
Jenn-Shing Chen
Tina Chow
Stefan Church
Douglas Clark
Christopher Coen
A. Louise Creagh
Michael Dixon
Andreas Dorda
Eric Faulques
Laurent Fenouil
Richard Fish
Albert Flounders
Raymond Fong
Hubert Gasteiger
Gregory Hiller
Richard Hix
Arlon Hunt
Mary Hunt
Caryn Jantzen
Jordan Kahn
Hyun-Ok Kim
C. Judson King III
Kimio Kinoshita
Judith Klinman
David Koch
Mark Konings
Gregory Klunder
Peter Kuhn
Susan Lauer
Scott Lynn
Anthony Mancuso
Xianglei Mao
Frank McLarnon
Douglas Miller
Kenneth Miller
Michael Moore
Stuart Naftel
Dan Neumann
Mark Nicholas
Jon Noring
Kenneth Oberhausen
Loree Poole
Lucy Randel
Bruce Rauhe
Ronald Reade
Paul Ridgway
Dorys Rojas
Ali Rostami
James Rudnicki
Richard Russo
David Schurig
Robert Selleck
Mark Shannon
Daniel Shapiro
Susan Sharfstein
Jonathan Spear
John Starr
Charlotte Standish
Craig Stevens
Kathryn Striebel
Jerome Thomas
Gavin Towler
Lisa Tung
Vincent Van Brunt
Jeffrey Weaver
Charles Wilke
Richard Williams

Contents

Introduction

The Energy Conversion and Storage Program applies chemistry and materials science principles to solve problems in 1) production of new synthetic fuels, 2) development of high-performance rechargeable batteries and fuel cells, 3) development of advanced thermochemical processes for energy conversion, 4) characterization of complex chemical processes, and 5) application of novel materials for energy conversion and transmission. Projects focus on transport-process principles, chemical kinetics, thermodynamics, separation processes, organic and physical chemistry, novel materials, and advanced methods of analysis.

Electrochemistry research aims to develop advanced power systems for electric vehicle and stationary energy storage applications. Topics include identification of new electrochemical couples for advanced rechargeable batteries, improvements in battery and fuel-cell materials, and the establishment of engineering principles applicable to electrochemical energy storage and conversion. Major emphasis is on applied research that will lead to superior performance and lower life-cycle costs.

Chemical Applications research includes topics such as separations, catalysis, fuels, and chemical analyses. Included in this program area are projects to develop improved, energy-efficient methods for processing waste streams from synfuel plants and coal gasifiers. Of particular interest are new techniques to remove compounds such as H_2S, NH_3 and phenols from effluents. Other research projects seek to identify and characterize the constituents of liquid fuel-system streams and to devise energy-efficient means for their separation. Also of current interest are the development of advanced methods for production of alcohols from hydrocarbon fuels, the application of modern chemical engineering principles to study processes in biological systems, the use of light-scattering techniques to characterize biomedical and biological processes, and the development of ultrasensitive spectroscopies for chemical analyses.

Materials Applications research includes the evaluation of the properties of advanced materials, as well as the development of novel preparation techniques. For example, the use of advanced techniques, such as sputtering and laser ablation, are being used to produce high-temperature superconducting films. Other projects include the application of novel microstructured materials to develop superinsulators; and the development of gas-particle suspensions for use in direct solar-thermal conversion processes and for the catalysis of important thermochemical reactions.

Electrochemistry

Technology Base Research Project for Electrochemical Energy Storage[1]

E.J. Cairns, K. Kinoshita, and F.R. McLarnon

Lawrence Berkeley Laboratory (LBL) is the lead center for management of the Technology Base Research (TBR) Project, supported by the Electric/Hybrid Propulsion Division of DOE's Office of Transportation Technologies. This project's research supports DOE development of electrochemical energy conversion systems for electric vehicles and stationary energy storage applications. The most promising electrochemical technologies are identified and transferred to industry and/or to another DOE program for further development and scale-up.

The TBR Project identifies new electrochemical couples for advanced batteries, determines the technical feasibility of the new couples, improves battery components and materials, establishes engineering principles applicable to electrochemical energy storage and conversion, and investigates fuel cell and metal/air systems for transportation applications. Major emphasis is given to applied research that will lead to superior performance and lower life-cycle costs.

The LBL scientists participating in the project are E.J. Cairns, K. Kinoshita, and F.R. McLarnon of the Applied Science Division; L.C. DeJonghe, J.W. Evans, R.H. Muller, J.S. Newman, P.N. Ross, and C.W. Tobias of the Materials Sciences Division.

Research projects conducted by subcontractors are described in the report *Technology Base Research Project for Electrochemical Energy Storage* (LBL-29155); in-house work is summarized in the next article and in the *Materials and Chemical Sciences Division 1989 Annual Report* (LBL-30432). Highlights of the subcontracted work follow.

EXPLORATORY RESEARCH

Efforts continue at Argonne National Laboratory (ANL) on two advanced high-temperature rechargeable battery systems: 1) LiAl/FeS_2 cells containing a dense upper-plateau FeS_2 electrode, a Li-Al electrode, and LiCl-LiBr-KBr electrolyte (m.p. 310°C); and 2) Na/β"-Al_2O_3/$NaAlCl_4$/$NiCl_2$ cells (Na/$NiCl_2$ cells). Over 400 h (175 cycles) of stable operation were achieved with a bipolar Li alloy/FeS_2 cell, which maintained acceptable integrity of the hermetic seal. ANL observed that comparable performance was obtained with an "electrolyte-starved" upper-plateau Li alloy/FeS_2 cell (compared to a flooded-electrolyte cell) by altering the electrolyte to a LiCl-rich composition (i.e., in mol%, 34 LiCl-32.5 LiBr-33.5 KBr). The addition of sulfur was observed to increase the utilization of Ni in Na/$NiCl_2$ cells by increasing the surface area and pore diameter of the Ni metal matrix. A composite of 35-wt% glass (Na_2O-Al_2O_3-B_2O_3-SiO_2) and β"-Al_2O_3 was identified which yielded acceptable resistivity (~25 ohm-cm) at 250°C for use as an alternative solid electrolyte in Na/metal chloride cells.

Projects are currently underway at the University of Pennsylvania (Penn) and SRI International (SRI) to develop rechargeable conducting-polymer cells. Penn is collaborating with the Energy Research Laboratory (Svendborg, Denmark) to characterize the electrochemical behavior of a new conducting polymer for rechargeable Li batteries. This polymer has the highest Li-ion conductivity at room temperature of any observed to date. Thermal analysis studies (DSC, TGA) indicate that the polymer is completely amorphous between -90°C and 200°C, and loses weight slowly between 40°C and 100°C. SRI has developed a Li-ion conducting polymer from a poly(ethyleneimine) derivative which also has one of the highest ionic conductivities (4×10^{-5} ohm^{-1} cm^{-1}) at room temperature reported so far.

APPLIED SCIENCE RESEARCH

Stanford University has observed that the positive electrode in Na/metal chloride cells limits the power output from cells of the present design. Evidence was found for time-dependent changes in the chloroaluminate molten salt.

Cyclic voltammetric studies at the Illinois Institute of Technology indicated that the deposition of Mo in FLINAK (LiF-NaF-KF molten salt) occurs by a 3-electron quasi-reversible process. Mo_2C coatings were successfully electrodeposited on the internal surface of container cans for Na/S cells, which showed encouraging results in tests at Chloride Silent Power Limited, England.

Brookhaven National Laboratory (BNL) has used extended x-ray absorption fine structure (EXAFS) to detect the waters of hydration and tetrahedral $Zn(OH)_4^=$ species, but no ion-pairing with alkali ions in saturated zincate solutions was observed. On the other hand, EXAFS revealed that considerable ion-pairing occurs in poly(ethylene oxide) (PEO) electrolytes, e.g., $ZnBr_2(PEO)_8$, $RbBr(PEO)_8$.

Spectroscopic techniques (e.g., Raman, XPS, thermal desorption) are being applied at Case Western Reserve University (CWRU) and Jackson State University (JSU) to characterize the surface of reactive alkali and Zn electrodes in organic and KOH electrolytes, respectively. CWRU has used Fourier transform infrared spectroscopy to detect the presence of carbonate species which form when Li reacts with CO_2 at low partial pressure, 2×10^{-7} torr. The increase in the intensity of the absorption band at 1450 cm^{-1} with exposure time to CO_2 indicates a gradual increase in the amount of carbonate that forms. JSU has observed by *in situ* Raman spectroscopy that the passive film formed on Zn electrodes in alkaline solution consists of $Zn(OH)_2$, which gradually transforms to ZnO when the potential is maintained in the passive region.

Johns Hopkins University has observed that the impurities (as high as 10,000 ppm and mostly water) in technical-grade propylene carbonate (PC) cause breakdown of the passive films that are formed on Fe and Ni in 0.5 M $LiClO_4$/PC.

AIR SYSTEMS RESEARCH

CWRU has observed that the pyrochlore, $Pb_2Ru_2O_{6.5}$, exhibits high activity for the 4-electron reduction of O_2 in alkaline solution. Unfortunately, in the anodic mode, the pyrochlore dissolves in the electrolyte In other studies, *ex situ* FTIR reflectance showed that Co tetramethoxyphenylporphyrin (CoTMPP) adsorbs on HOPG in different orientations, depending on the preparative procedure.

Metal Air Technology Systems International (MATSI) has demonstrated that over 500 charge/discharge cycles can be obtained for Zn deposition in a reticulated Cu-foam structure. Zinc loadings of 100 mAh/cm^2 can be routinely deposited without dendrite formation.

Los Alamos National Laboratory (LANL) achieved current densities of over 2 A/cm^2 in polymer-electrolyte membrane fuel cells with 50-μm-thick Nafion. Performance losses at higher current densities are attributed to an increase in cathode overpotential. The anode performance with fuels which contain CO was observed to be a strong function of the fuel utilization. At high rates of fuel flow (i.e., low utilization) the performance degradation caused by 100-ppm CO is severe, whereas at low flow rates (i.e., high utilization) the performance degrades slowly. These results suggest that the improvement at low flow rates may be caused by the interaction of CO and O_2 which permeates through the membrane.

BNL has investigated underpotential deposited (UPD) Cu and Pb on Pt as an electrocatalyst for methanol oxidation. X-ray absorption near-edge spectroscopy (XANES) studies indicated that these UPD species were present in the nonmetallic state. EXAFS studies of pyrolyzed Fe-TMPP (900 °C) and Co-TMPP (800 °C) showed no evidence of any nitrogen present. These findings contradict other hypotheses on the role of nitrogen in O_2 reduction on pyrolyzed macrocycle electrocatalysts.

Advanced Electrode Research[1]

E.J. Cairns, F.R. McLarnon, T.C. Adler, H. Gasteiger, K.G. Miller, S.A. Naftel, B. Rauhe, P. Ridgway, J. Rudnicki, and J. Weaver

We have been studying the behavior of electrodes used in advanced secondary batteries and fuel cells currently under development for energy storage applications. In addition, we have been investigating practical means for improving the performance and lifetimes of these batteries and fuel cells. Systems of current interest include ambient-temperature, alkaline-electrolyte rechargeable cells with Zn electrodes (Zn/air, Zn/NiOOH); rechargeable high-temperature cells (Li/S, LiAl/FeS_2, Na/S and Na/$NiCl_2$); and fuel cells. We study life-limiting and performance-limiting phenomena under realistic cell operating conditions.

ALKALINE ZINC ELECTRODES

Rechargeable alkaline Zn/air and Zn/NiOOH cells can be designed to deliver high specific energy and specific power, but these cells typically have short lifetimes. The high solubility of Zn species in alkaline electrolytes tends to enhance the various physico-chemical processes (e.g., active material redistribution and filamentary Zn growths) that degrade the cell's capacity and limit its life. Through modeling and experimental investigations, we have been studying the complex transport processes in Zn electrodes. We have also been characterizing various methods to reduce Zn species solubility, and we have extended the lifetime of the Zn electrode.

A Mathematical Model of the Rechargeable Zn/NiOOH Cell[1]

K.G. Miller, E.J. Cairns, and R. F. McLarnon

Our one-dimensional, time-dependent model of the Zn/NiOOH cell has been used to characterize the transport of soluble Zn species from the Zn electrode to the NiOOH electrode. The uptake of Zn by the NiOOH electrode has been found to be an important process in the rate and extent of shape change. There is experimental evidence that about 25% of the initial amount of Zn active material migrates from the Zn electrode to the Ni electrode during the first 2-3 cycles. The form in which it exists is not well understood. The mathematical model accounted for this phenomenon by allowing 25% of the initial quantity of Zn to be incorporated in the NiOOH electrode, and then allowing 0-50% of that amount to leave the NiOOH electrode on charge and to be redeposited on discharge. The 50% figure was selected considering experimental observations, and the deposition/dissolution was assumed to occur at a constant rate. It was found that the greater the amount of the Zn that was allowed to leave and reenter the NiOOH electrode, the faster the rate and extent of shape change, with Zn material moving from the center toward the edges of the Zn electrode.

In Situ Characterization of Zinc Electrode Processes[1]

J. Weaver, E.J. Cairns, and R. F. McLarnon

In our research directed at characterizing Zn electrodes, we investigated mass transfer phenomena within a model pore. The model pore used in our work simulated a microscopic pore existing in the electrode of a rechargeable Zn battery. Our investigations employed optical probe-beam deflection as an *in situ* technique to measure electrolyte concentration gradients in a model pore. This technique was complemented by optical microscopy to study surface oxide formation, precipitation, dendrite formation, and other phenomena in the model pore. During 1990 we developed a two-dimensional mathematical model of the non-linear, secondary current and potential distributions within the model pore. The numerical results of the model provided information about the reaction distribution along the model pore electrode and thus help determine how the active material in a porous electrode will be utilized during charge-discharge cycling. These calculations also provided the boundary conditions needed to calculate electrolyte concentration distributions in the model pore cell.

A one-dimensional model was used for preliminary interpretation of the model pore experimental data. However, our data showed that the concentration gradients varied strongly in two dimensions, therefore an adequate mathematical model must include two spatial variables. A two-dimensional mathematical model of mass-transfer processes in the model pore cell has now been developed. The mass-transfer model incorporates the abovementioned current-potential distribution model, and it allows direct, quantitative calculations of the concentrations of the electrolyte species.

The results from the two mathematical models were in good quantitative agreement with our experimental data. The probe-beam deflection technique is therefore proven as a very useful technique for the investigation of mass transfer phenomena within a model pore. The good agreement between theory and experiment also suggests that the mathematical models adequately accounted for the physical and chemical processes occurring within an electrode pore. A logical extension of our theoretical work is to develop models of more-realistic pore geometries and ultimately develop a full electrode model comprised of randomly distributed pores.

Investigations of Methods to Improve the Lifetime of the Zinc/Nickel Oxide Cell[1]

T.C. Adler, E.J. Cairns, and F.R. McLarnon

We have now virtually eliminated the major problems restricting the cycle-life performance of 1.35-Ah Zn/KOH/NiOOH cells: 1) loss and redistribution of Zn electrode active material (shape-change); 2) Zn electrode dendritic growths that eventually lead to cell shorting and failure; and 3) frequent reformation of vented cells caused by inefficiency of the NiOOH electrode.

The shape-change problem has been overcome by the use of electrolyte compositions having low zincate solubility. In flooded, vented cells cycled at 100% depth-of-discharge, a cell with 2.5M KOH - 2.5M K_2CO_3 - 0.5M LiOH electrolyte retained 60% of its initial capacity after 470 cycles, and a cell with 3.5M KOH - 3.3M KF electrolyte has retained 70% of its initial capacity after 820 cycles. *In situ* x-ray photographs of these cells revealed only moderate Zn redistribution, but the cells occasionally experienced dendritic shorts. These cells exhibited peak specific powers ranging from 200 to 300 W/kg, which is adequate for electric vehicle applications.

Dendritic shorting and reformation problems were solved by the use of a sealed, electrolyte-starved cell configuration in which the cell is sealed under vacuum, and the quantity of electrolyte is limited to that which fills the pores of the electrodes and separator materials. As the cell is cycled the inefficiency of the NiOOH electrode produces an O_2-enriched atmosphere in the cell. The O_2 not only reacts with the Zn metal in the negative electrode, thereby eliminating the need for reformation, but also scavenges incipient Zn dendrites. In this sealed, electrolyte-starved configuration, a 6.8M KOH - 0.5M LiOH standard electrolyte cell reached 190 deep-discharge cycles, which is a 50% improvement over flooded, vented control cells. Another sealed, electrolyte-starved cell with low-zinc-solubility electrolyte retained 80% of its original capacity after 290 deep-discharge cycles, and exhibited almost no shape-change. Both of these cells were essentially maintenance-free, showed no dendrites, and required no reformation. These characteristics are ideal for electric-vehicle and other applications.

HIGH-TEMPERATURE CELLS

The high-temperature Na/S cell offers very good performance, and recent improvements to the process for manufacturing the ceramic β''-Al_2O_3 electrolytes indicate that acceptable cell lifetimes may be realized. However, the performance of the sulfur electrode has not been optimized, and the phenomena which govern its operation are poorly understood. In addition, Na/S cells cannot tolerate overcharge and overdischarge, a problem that complicates the design of cell-string configurations for battery applications. Ongoing work is aimed at developing and confirming an advanced mathematical model of the sulfur electrode, and exploring variants of Na/S cells that may exhibit improved performance and active material utilization.

Mathematical Modeling of the Sodium/Sulfur Cell[1]

S.A. Naftel, F.R. McLarnon, and E.J. Cairns

A comprehensive model of the sulfur electrode in Na/S cells has been developed. The cell being modeled is of the tubular central-sodium type, and includes a thin layer of α-Al_2O_3 felt around the β''-Al_2O_3 solid electrolyte in order to prevent deposition of sulfur on the solid electrolyte during cell charge. The model consists of a set of non-linear Partial Differential Equations (PDE's) which describes the processes of diffusion, migration, and convection which take place during the operation of such a cell. Linearization of these highly nonlinear equations and their boundary conditions has been accomplished by implementation of a symbolic equation manipulator, written in *Mathematica*. The *Mathematica* program automatically generates the corresponding banded matrices used in the Newman-IAD technique for solving time-dependent PDE's. This work results in a tremendous reduction of the tedious effort necessary to linearize the PDE's, and to generate the corresponding matrices necessary for numerical solution. Solution of the linearized equations is presently being performed on the UC Berkeley Cray X/MP computer via implementation of the Newman-IAD method, which is a numerical technique for solving the finite-difference equations which arise in the solution of second-order linear PDE's.

Due to the mathematical complexity of the system, which involves the simultaneous solution of both elliptic and parabolic equations, with the character (elliptic or parabolic) at each point dependent upon the phases present, the numerical solution has been split into two stages: 1) solution of the system in the one-phase region, and 2) solution of the system in the two-phase region. We are currently near completion of (1) above. Significant results are expected within the next six months. An attempt will be made to predict the effect of various charge-discharge regimens upon cell operation.

Evaluation of Sodium/Sulfur-Phosphorus Cells[1]

P.L. Ridgway, F.R. McLarnon, and E.J. Cairns

The addition of phosphorus to the sulfur cathode in the Na/S cell may improve power output by reducing Na^+-ion transport resistance. We anticipate that the long-chain sodium polysulfides which form in standard sulfur electrodes during discharge will be modified to lower-molecular-weight species by phosphorus, which may act as a molecular chain terminator in this system. This would decrease the viscosity in the cathode melt, allowing faster transport of Na^+ ions in the melt, thereby decreasing cell overpotential and increasing its power output.

During 1990 we continued to develop an experimental cell which will permit the evaluation of optimal P/S ratios via equilibrium EMF measurements at temperatures up to 500°C. The cell uses solid ceramic β''-Al_2O_3 electrolyte, and is constructed much like standard Na/S cells. Most of our effort has been directed at improving the cell design so that a hermetic seal is maintained at elevated temperatures.

FUEL CELLS

Fuel cells can be designed to exhibit acceptable lifetimes for a number of applications, and the use of fuel cells for transportation purposes is of particular interest to this program. The performance of the O_2 electrode in fuel cells requires improvement, and the development of an efficient direct-methanol fuel cell would represent a major advance over reformed-hydrocarbon fuel cells.

Application of Photothermal Deflection Spectroscopy to Characterize Direct Methanol Electrooxidation[1]

J. Rudnicki, F.R. McLarnon, and E.J. Cairns

We are developing Photothermal Deflection Spectroscopy (PDS) as a powerful *in situ* technique for the study of electrochemical interfaces. PDS is a sensitive technique which measures the absorption spectrum of the electrode surface and simultaneously detects the concentration gradients formed in the electrolyte. The absorption spectrum can help identify reaction intermediates, which in turn help to determine the pathway by which the reaction occurs. The electrolyte concentration gradients contain information about the diffusion of reactants and products to and from the electrode. The sensitivity of these measurements is sufficiently high to detect reactions involving a single layer of molecules on the electrode surface.

The rate-limiting step in the direct electrochemical oxidation of CH_3OH appears to be the transfer of O_2 from the electrolyte to the Pt catalyst where it can react with CH_3OH to form CO_2. This overall reaction is very slow at the operating potential of a CH_3OH anode in a fuel cell. We have been studying the process by which oxide layers form on Pt so that this rate-limiting step can be better understood. Our initial focus has been the measurement of electrolyte concentration gradients that accompany the formation and removal of oxide films on Pt. Our measurements suggest that two phenomena play important roles in Pt oxide film formation: 1) the movement of H_2O to and from the electrode, and 2) a non-electrochemical reaction. Water transport is rarely considered in mechanistic studies, however PDS is sufficiently sensitive to detect small changes in H_2O concentration near the electrode surface. The ability to detect a non-electrochemical reaction is a powerful feature of PDS. The electrochemist's standard tool, the potentiostat, can detect only electrochemical reactions.

Mathematical models of several reaction pathways were used to predict the concentration gradients, and the corresponding electrolyte refractive-index gradients. These predictions were then compared to experimental data. Among the reaction pathways evaluated, one pathway is strongly preferred: a two-reaction pathway whereby $Pt(OH)_2$ is formed by an electrochemical step and dehydrates by a chemical step to form PtO. Investigation of this reaction pathway is continuing, however, it has an important implication for direct CH_3OH electrooxidation: the dehydration reaction removes oxygen from the electrode surface, which is just the opposite of what is needed for CH_3OH oxidation. Slowing the rate of hydroxide dehydration could improve the overall electrochemical reaction rate for CH_3OH oxidation.

Characterization of Direct Methanol Electrooxidation[1]

H. Gasteiger, F.R. McLarnon, and E.J. Cairns

Fuel cells based on the electrooxidation of CH_3OH are an environmentally benign alternative to internal-combustion engines, promising electric vehicles with range and acceleration characteristics similar to vehicles in use today. However, poorly understood reactions poison the direct electrooxidation of CH_3OH at fuel cell anodes, therefore this kind of fuel cell is not economically feasible. There has been a world-wide effort to identify electrocatalyst-electrolyte combinations which promote higher electrooxidation rates and avoid the poisoning problem. The best reaction rate enhancement has been achieved with Pt-Ru alloy electrodes, and many different mechanisms have been hypothesized to account for its improved activity. Our research, therefore, is directed toward two goals:

First, a systematic performance assessment of Pt-Ru alloys in several acidic electrolytes will be carried out. The reported difference between the alloy bulk composition and its surface composition, which has been neglected in most former investigations, will be investigated. Auger electron spectroscopy (AES) is envisaged as an appropriate analytic tool.

Second, PDS will be used for the *in situ* detection of the

absorption of infrared radiation by surface species (submonolayer coverages) via the deflection of a small laser beam traversing parallel to the electrode. Recently, we have been improving the precision of the optical alignment procedure of the system, which is needed to make PDS a quantitative technique. Concurrently, an analytical mathematical model describing PDS responses has been developed. Our present efforts are directed at advancing PDS into the infrared region of the spectrum, and a thin-layer electrochemical cell has been built for this purpose. Thus, we hope to be able to elucidate the "true" mechanism of methanol electrooxidation, and develop the ability to "intelligently" design better catalysts.

Effect of Electrocatalyst and Electrolyte Composition on Methanol/Air Fuel Cell Performance[1]

B. Rauhe, F.R. McLarnon, and E.J. Cairns

Poisoning of the anodic reaction is the major impediment to the advancement of the direct methanol fuel cell (DMFC) as an efficient power source for stationary and transportation applications. Certain of these poisons occur as intermediate species during the oxidation of CH_3OH to CO_2 and H_2O. These species increase anodic overpotentials and thereby reduce fuel cell performance.

The standard/primary catalyst used in aqueous fuel cells, Pt, is ineffective in oxidizing these intermediates/poisons at useful potentials. However, the additions of certain metals (e.g., Ru) to the Pt catalyst have shown promise in reducing anodic overpotentials. The benefits of using of Ru as a co-catalyst to Pt derive from its apparent efficacy in reducing the oxidation potentials of the poisoning intermediate species.

In the present work, various ratios and amounts of Pt and Ru, supported on graphitized carbon black, will be examined for efficiency in increasing the performance of gas diffusion electrodes (GDEs) with vaporized methanol as fuel. Experiments will be carried out at elevated temperatures (70-130 °C) in aqueous carbonate electrolytes of various ionic strengths. Catalysts will be prepared by co-deposition from aqueous solutions of metal salts and/or acids onto graphitized carbon black (Cabot XC-72).

The physical structure of the GDEs will be varied to determine its relationship to fuel cell performance. Electrodes will be prepared by pressing a catalyzed graphite slurry (containing ~30% PTFE) onto a hydrophilic graphite sheet, which acts as a physical support for the catalyzed graphite as well as the gas diffusion layer and the current collector.

References

McLarnon FR, Cairns EJ. The secondary alkaline zinc electrode. *J. Electrochem. Soc.* 1991; 138: 645.

Isaacson MJ, McLarnon FR, Cairns EJ. Zinc electrode rest potentials in concentrated KOH-$K_2Zn(OH)_4$ electrolytes. *J. Electrochem. Soc.* 1990; 137: 2361.

Isaacson MJ, McLarnon FR, Cairns EJ. Current density and ZnO precipitation-dissolution distributions in Zn-ZnO porous electrodes and their effect on material redistribution: a two-dimensional model. *J. Electrochem. Soc.* 1990; 137: 2014.

Weaver J, McLarnon FR, Cairns EJ. Investigation of a model pore zinc electrode using the probe beam deflection method. Paper No. FR-10. Presented at the 41st Meeting of the International Society of Electrochemistry, Prague, Czechoslovakia, 1990.

Adler TC, McLarnon FR, Cairns EJ. Advances in the cycle-life performance of Zn/NiOOH cells. Paper No. 100. Presented at the 178th Meeting of the Electrochemical Society, Seattle, WA, 1990.

Striebel KA, McLarnon FR, Cairns EJ. Oxygen reduction on Pt in aqueous K_2CO_3 and KOH. *J. Electrochem. Soc.* 1990; 137: 3351.

Striebel KA, McLarnon FR, Cairns EJ. Fuel cell studies in aqueous K_2CO_3 and KOH. *J. Electrochem. Soc.* 1990; 137: 3360.

Rudnicki JD, McLarnon FR, Cairns EJ. *In situ* characterization of electrode processes by photothermal deflection spectroscopy. In: Varma R, Selman JR. eds., *Techniques for Characterization of Electrodes and Electrochemical Processes*. New York: John Wiley and Sons, 1991.

Haas O, Rudnicki J, McLarnon FR, Cairns EJ. Mechanistic investigation of redox polymer-coated electrodes using probe-beam deflection and cyclic voltammetry. *J. Chem. Soc. Faraday Trans.* 1991; 87(7): 939.

Advanced Rechargeable Zinc Cells[5, 6]

E.J. Cairns, F.R. McLarnon, T.C. Adler, J.-S. Chen, and K.A. Striebel

Zinc is the most commonly used battery electrode because of its low equilibrium potential, electrochemical reversibility, compatibility with aqueous electrolytes, low equivalent weight, high specific energy and volumetric energy density, abundance, low cost, low toxicity, and ease of handling. Zinc has been considered for use as the negative active material in several rechargeable batteries; however, short lifetimes have severely limited the use of such batteries. LBL research efforts have resulted in major improvements to the lifetime of the rechargeable Zn electrode in alkaline electrolytes, and efforts are underway to apply these improvements in rechargeable Zn/air, Zn/NiOOH and Zn/AgO cells.

Rechargeable Zinc/Air Cells for Electric Vehicles[5]

K.A. Striebel, F.R. McLarnon, and E.J. Cairns

The electrically rechargeable Zn/air cell is being evaluated for its suitability to power an electric vehicle. This cell exhibits a high theoretical specific energy and an adequate specific power and volumetric power density at ambient temperatures, and it is superior to other rechargeable batteries in the areas of safety, abuse resistance, environmental impact and the use of key resources. The reticulated-Zn flow-through electrode has been tested for as many as 800 cycles with essentially no Zn active material redistribution (shape change) which is the most prevalent failure mechanism of the pasted Zn electrode.

We are studying the performance of 5 × 5 cm reticulated (foam) substrate electrodes coupled with two air electrodes in a monopolar arrangement. Forced convection of 45 wt% KOH electrolyte tangentially through the 0.6-cm thick electrode carries dissolved Zn to the foam substrate during charge and away from it during discharge. Due to the absence of a suitable bifunctional air electrode, Ni expanded-mesh oxygen-evolving electrodes are used during charge of the Zn electrode and cobalt tetramethoxyphenylporphyrin (CoTMPP)-catalyzed air electrodes are used during discharge.

A computer-controlled system has been assembled to test the performance of these cells under the Simplified Federal Urban Driving Schedule (SFUDS) power profile. Individual electrode performances are measured with the aid of a reference electrode. Comparisons are made between the SFUDS data and steady-state performance data in order to identify potential problems encountered with the SFUDS profile that cannot be anticipated from steady-state results.

Future work will involve evaluation of novel separator materials for this cell, and an alternative three-electrode arrangement will be considered as a means to avoid the use of a bifunctional air electrode.

Development of 22-Ah Zinc/Nickel Oxide Cells[5]

T.C. Adler, F.R. McLarnon, and E.J. Cairns

We are now scaling up to 22-Ah Zn/KOH/NiOOH cells containing three negative and four positive electrodes. A new 486 PC-based cell cycling system is being developed to permit cycle-life tests of the large cells using the SFUDS discharge power profile. Thus both cell size and operating parameters will more closely simulate actual electric vehicle requirements.

Improved Lifetime of Zinc/Silver Oxide Cells[6]

J.-S. Chen, T.C. Adler, K.A. Striebel, F.R. McLarnon, and E.J. Cairns

Active material redistribution (shape change) of the Zn electrode is a primary limiting factor in the life of Zn/AgO secondary cells. Advanced Zn electrode and alkaline electrolyte compositions are being studied to determine their ability to extend the cycle-life performance of Zn/AgO cells. Zinc electrodes will be fabricated by pressure-bonding two cakes containing (typically) 93 wt% ZnO, 2 wt% PbO,4 wt% PTFE and 1 wt% newsprint to the sides of a Pb-plated Cu expanded-metal mesh current collector. Reduced-alkalinity electrolytes have been shown to reduce the rate and extent of shape change of Zn electrodes during cycle-life testing of Zn/NiOOH cells. Cells using 2.5M KOH - 2.5M K_2CO_3 - 0.5M LiOH, 6.8M KOH - 1.75M K_2CO_3 - 0.5 M LiOH and 3.5M KOH - 3.3M KF have exceeded 300 deep-discharge cycles while maintaining more than 60% of their initial capacities. The addition of $Ca(OH)_2$ to the Zn electrode can also slow the rate and extent of Zn redistribution. Cells constructed with electrodes of 25 mol% Ca showed the best cycle-life performance among tests of cells with different contents of $Ca(OH)_2$. We will apply these results to Zn/AgO cells, aiming toward a goal of more than 300 cycles with less than 25% capacity loss.

Chemical Applications

Removal of H_2S Using Metal Salts[7]

N.M. Barthelemy, D.J. Koch, G.P. Towler, and S. Lynn

The goal of this project is to do the preliminary research needed to determine the technical and economic feasibility of two novel methods for removing sulfur compounds from a coal gas very completely and with very high selectivity. The potential processes convert the sulfur compounds either to elemental sulfur or to calcium sulfate and causes minimal loss of work potential in the coal gas.

Treatment at the Adiabatic Saturation Temperature

In the proposed process the effluent from a coal gasifier is first quenched adiabatically (300 to 500 psia and 350° to 450°F) and scrubbed free of particulates, ammonia and HCl. The hot wet gas is then contacted with a solution of either ferrous or zinc sulfate, either of which reacts with H_2S to form the insoluble sulfide and bisulfate by Reaction (1):

$$2\ MeSO_4 + H_2S \rightarrow MeS + Me(HSO_4)_2 \quad (1)$$

The method of contacting would probably be by venturi scrubber.

The acidic slurry of metal sulfide is cooled to about 200° to 250°F and then mixed with a recycled aqueous stream (see below) containing acidic ferric sulfate, which reacts with part of the MeS by Reaction (2).

$$MeS + 2\ Fe^{3+} \rightarrow Me^{2+} + S + 2\ Fe^{2+} \quad (2)$$

The reaction vessel serves also as a settler. The overflow is regenerated metal sulfate solution. The underflow contains a slurry of solid or liquid sulfur in the same solution. The slurry, if solid, is heated just above the melting point of sulfur (240°F), and the sulfur is coalesced and decanted. As was noted above, the aqueous stream from the decanter is recycled to an absorber in which ferrous sulfate is reoxidized the ferric state with air.

During FY 1990 some progress was made in studying the kinetics of the absorption of H_2S by metal sulfates. Absorption is done by sparging a sour gas into a solution of the absorbent in a vessel under fixed conditions of solution volume, agitation and gas dispersion. The rate of absorption into a solution of sodium hydroxide is used as the base case since the reaction of H_2S with NaOH is known to be virtually instantaneous. The pH of the sulfate solutions is buffered at about 2. The rate of absorption by zinc sulfate is limited by the kinetics of ZnS crystallization. The rate improves at higher temperature and also becomes faster as the surface area increases, i.e., as the reaction proceeds. The kinetics of CuS crystallization appears to be quite rapid, possibly because the solubility of CuS is much less than the solubility of ZnS. Copper sulfate solutions appear to absorb H_2S as rapidly as NaOH solutions of the same concentration.

Modified Heat-Recovery System

The exhaust gas leaving a combustion turbine is typically at a temperature of 500-600°C (900-1100°F). Heat may be recovered from this gas by raising steam. In a power plant this steam may be employed in a steam turbine (combined cycle) or may be injected into the combustion chamber to reduce the excess air required to control the temperature of the gas entering the turbine. A steam-injected system can approach the thermal efficiency of a combined-cycle system at lower capital cost.

At a given inlet temperature and pressure the power generated by a turbine increases in almost exact proportion with the molar flow of gas through the turbine. Quenching the fuel gas with water increases its molar flow but decreases its temperature. The latter effect predominates if water at ambient temperature is used for the quench, so that the total flow of gas through the turbine is reduced. However, if low-temperature heat (energy at too low a temperature to generate steam at the turbine pressure) is used to preheat the quench water, the molar flow of quench water can be increased and with it the thermal efficiency. At the cost of approximately doubling the heat-exchange area in the heat-recovery unit following the combustion turbine, which appears to be economically justified, this system actually increases the thermal efficiency relative to a conventional steam-injected turbine.

This approach is also attractive when coupled with a

system of hot-gas clean-up. Such systems typically would be operated at a temperature above that of the turbine exhaust, and hence the fuel gas would then not be used to recover sensible heat from the exhaust. The combustion air, including a large fraction of the air flow to the coal gasifier, would still be quenched and used for heat recovery. The remaining sensible heat of the exhaust would be used to preheat this quench water.

The computer modeling of the heat-recovery system described above is nearly completed. As expected, a hot-gas clean-up process leads to improved thermal efficiency for all types of gasifiers, assuming that the materials problems associated with the control of the gas flow at high temperature can be resolved satisfactorily. This study will be completed during FY 1991.

Sorption of H_2S with Limestone

The second method of gas clean-up uses limestone (rather than lime) to absorb H_2S and HCl, and to filter particulates. A consideration of the chemistry of the H_2S removal shows there are three reactions to consider:

$$CaCO_3 + H_2S \leftrightarrow CaS + H_2O + CO_2 \quad (1)$$

$$CaCO_3 \leftrightarrow CaO + CO_2 \quad (2)$$

$$CaO + H_2S \leftrightarrow CaS + H_2O \quad (3)$$

Reaction (1) is slightly endothermic (+25.4 kcal) and is thermodynamically favorable even at the relatively low temperature of 1000K (1340°F). It becomes more favorable with increasing temperature. Reaction (2) has a threshold temperature that depends on the partial pressure of CO_2. For the coal gas from an air-blown fluid-bed gasifier at 500 psia the temperature is about 1273K (1830°F). Reaction (3) is slightly exothermic (-15.2 kcal) and becomes increasingly less favorable at temperatures above 1273K.

The rate of sorption of H_2S by limestone is limited by both kinetics and equilibrium. Equilibrium calculations indicate that the optimal temperature range is relatively narrow and just under the calcination temperature of the limestone. On the other hand, the kinetics of sorption is drastically reduced by sintering, so operation below the sintering temperature is essential. A primary goal of this research will be the determination of the kinetics of the sorption reaction as a function of temperature and gas composition.

Once formed, calcium sulfide must be disposed of by the most economical method that is also environmentally sound. It may be oxidized to calcium sulfate or converted to calcium carbonate and elemental sulfur. A second goal of this research will be the determination of the relative merits of these two approaches.

References

Russell JV, Lynn S. *Development and Evaluation of a Superior Heat-Recovery Design for Gas-Turbine Systems Using Gasified Coal.* Lawrence Berkeley Laboratory Report No. LBL-27954, August 1989.

Higdon CR, Louks BM, Lynn S. A novel heat-recovery process for improving the thermal efficiency of gas turbines in electric power generation. In: *Proceedings of the American Power Conference* 1990; 52:216.

Organometallic Synthesis and Catalysis Studies[10,13]

R.H. Fish, E. Baralt, H-S. Kim, R.H. Fong, A. Tran, S.J. Smith, M.S. Konings, K.J. Oberhausen, W.M. Yu, G. Christou, J.B. Vincent, D.K. Coggin, and R.M. Buchanan

The focus of the Organometallic Chemistry Group is in two areas of research. The first area includes the bonding studies of polynuclear heteroaromatic nitrogen (PHN), model coal compounds with organorhodium and organoruthenium complexes, and the chemistry associated with these nitrogen or π-bonded complexes. Homogeneous catalysis studies on the regioselective hydrogenation of PHN compounds utilizing the above-mentioned complexes as catalyst precursors is also an important goal of this program. The second area of research is biomimetic catalysis, which is directed toward the synthesis and catalytic activity of mimics of methane monooxygenase enzymes. The conversion of small hydrocarbons, such as methane, to their respective alcohols, i.e., methanol, is the major goal of this project, and also includes the mechanistic aspects of these oxidation reactions.

Bonding of Mono- and Polynuclear Heteroaromatic Nitrogen Ligands to (η^5Pentamethylcyclopenta-dienyl) rhodium Dication: Structure-Reactivity Relationships in the Formation of Nitrogen (η^1) versus π (η^5, η^6) Complexes and Competition Studies of the Ligands for the Rhodium Metal Center[10]

R.H. Fish, E. Baralt, and H-S. Kim

The reactions of 4-methylpyridine, **1**; 3-methylpyridine, **2**; 2-methylpyridine, **3**; 3,5-dimethylpyridine, **4**; 2,4-dimethylpyridine, **5**; 2,4,6-trimethylpyridine, **6**; N-methylpyrrole, **7**; quinoline, **8**; isoquinoline, **9**; 2-methylquinoline, **10**; 1,2,3,4-tetrahydroquinoline, **11**; N-methylindole, **12**; acridine, **13**; phenanthridine, **14**; 5,6-benzoquinoline, **15**; and 7,8-benzoquinoline, **16**, with (η^5-pentamethylcyclopentadienyl)rhodium dicationic complexes [$Cp^*Rh(CH_3CN)_3X_2$ or $Cp^*Rh([CH_3]_2CO)_3X_2$; X = PF_6 or BF_4] were studied to ascertain how structure influenced the reactivity of ligands **1-16**, to provide nitrogen (N) versus π-bonded Cp^*Rh^{2+} complexes. Ligands **1-5**, **8**, **9**, and **13-16** were found to form N(η^1) bonded rhodium complexes, while ligands **6**, **7**, **11**, and **12** preferred π(η^5, η^6)-coordination. Ligand **10** formed the N(η^1)-bonded complex with $[Cp^*Rh(CH_3CN)_3]^{2+}$ and an ~1:1 mixture of N(η^1)- and π(η^6)-bonded complexes with the $(CH_3)_2CO$ derivative. The order of competitive reactivity with ligands **3**, **6**, **8-11**, **14-16** for the rhodium metal center was found to be: **9** (N) > **11** (π) > **8** (N) > **3** (N) > **10** (N) > **14** (N) > **15**(N) ~**16** (N) > **6**(π) ~ **7**(π).

The Bonding Mode of Nitrogen Heterocyclic Ligands to (η^5-Cyclopentadienyl)ruthenium Cation and Reactivity Studies of the Nitrogen- and π-Bonded Complexes: Mechanistic Aspects of a Nitrogen-to-π Rearrangement[10]

R.H. Fish, H-S. Kim, and R.H. Fong

Nitrogen heterocyclic ligands (pyridine, **1**; 2-methylpyridine, **2**; 2,4-dimethylpyridine, **3**; 2,4,6-trimethylpyridine, **4**; quinoline, **5**; isoquinoline, **6**; 2-methylquinoline, **7**; and 1,2,3,4-tetrahydroquinoline, **8**) were reacted with (η^5-cyclopentadienyl)ruthenium cation [$CpRu(CH_3CN)_3(PF_6)$] to ascertain the mode of bonding as a function of structure, i.e., nitrogen (η^1, N) versus $\pi(\eta^6)$-bonding. Ligands **1-3**, **5**, and **6** formed N-bonded complexes, while **4**, **7**, and **8** only formed π-bonded complexes. Thus, it appears that steric and electronic effects influence the bonding mode of nitrogen heterocyclic compounds to $CpRu^+$. An interesting $N(\eta^1)$-to-$\pi(\eta^6)$ rearrangement occurred with the N-bonded $CpRu^+$ complexes of ligands **2**, **3**, and **5**, and mechanistic aspects were studied by 1H NMR spectroscopy.

Heteroaromatic Nitrogen Ligand Studies with (η^5-Penta-methylcyclopentadienyl) ruthenium Cation: η^1, N and $\eta^6(\pi)$ Bonding Modes and Factors that Influence a Nitrogen-to-π Rearrangement[10]

R.H. Fish, R.H. Fong, A. Tran, and E. Baralt

The reactions of (η^5-pentamethylcyclopentadienyl) ruthenium trisacetonitrile cationic complex, [$Cp^*Ru(CH_3CN)_3$] (OTf), with pyridine, **1**; 2-methylpyridine, **2**; and quinoline, **3**, were studied to ascertain bonding modes as a function of heteroaromatic nitrogen ligand structure. Ligand **1** bonds η^1, N and forms mono- or trispyridine complexes with $[Cp^*Ru(CH_3CN)_3]^+$ depending on ligand concentration. Ligand **2** only forms an η^6 complex with $[Cp^*Ru(CH_3CN)_3]^+$, while ligand **3** also forms an η^6 complex, but with the benzo ring not the nitrogen ring. In the presence of excess pyridine, the complexed CH_3CN ligands are fully displaced to form $[Cp^*Ru(\eta^1, N\text{-pyridine})_3]^+$, while in the presence of excess **2** or **3** only the $[Cp^*Ru(\eta^1,N)(CH_3CN)_2]^+$ complexes are formed. The latter $[Cp^*Ru(\eta^1, N)(CH_3CN)_2]^+$ complexes with ligands **2** and **3** were not isolated; rather, they undergo a rapid nitrogen (N)-to-π rearrangement to the corresponding η^6 complexes, $[Cp^*Ru(\eta^6\text{-2-methylpyridine or quinoline})]^+$. The isolation of $[Cp^*Ru(\eta^1, N\text{-pyridine})(CH_3CN)_2]^+$ and its conversion to $[Cp^*Ru(\eta^6\text{-pyridine})]^+$ clearly demonstrates the pathway to the η^6 complexes. Ligand exchange reactions of $[Cp^*Ru(\eta^6\text{-pyridine})]^+$ with CD_3CN and pyridine-d_5 show facile replacement of the η^6-bonded pyridine, while the former result with CD_3CN ligand exchange proves that the N-to-π-rearrangement is not reversible.

Homogeneous Catalytic Hydrogenation, 5: Regioselective Hydrogenation of Mono- and Polynuclear Heteroaromatic Compounds Using the (η^5-Pentamethylcyclopentadienyl) rhodium Trisacetonitrile Dication as the Catalyst Precursor[10]

R.H. Fish, E. Baralt, and S.J. Smith

The regioselective hydrogenation of representative mono- and polynuclear heteroaromatic nitrogen and sulfur model coal compounds such as 2-methylpyridine, **1**; quinoline, **2**; 2-methylquinoline, **3**; 5,6- and 7,8-benzoquinolines, **4** and **5**; acridine, **6**; and benzothiophene, **7**, was studied with (η^5-pentamethylcyclopentadienyl)rhodium trisacetonitrile dicationic complex $[Cp^*Rh(CH_3CN)_3]^{2+}$ as the catalyst precursor. The order of relative rates as a function of structure was found to be **5** >>> **6** > **2** > **4** > **3** > **7** >> **1**. Replacement of H_2 with D_2 provided information on several of the mechanistic aspects of these selective hydrogenation reactions with compounds **2** and **7** as examples.

Biomimetic Oxidation Studies, 5: Mechanistic Aspects of C-H Bond Activation with Fe, Fe_2O, and Fe_4O_2 Complexes in the Presence of Hydrogen Peroxide[10]

R.H. Fish, M.S. Konings, K.J. Oberhausen, R.H. Fong, W.M. Yu, G. Christou, J.B. Vincent, D.K. Coggin, and R.M. Buchanan

Activation of cyclohexane with iron complexes, $Fe_2O(OAc)_2(bipy)_2Cl_2$, **1**; $Fe_4O_2(OAc)_7(bipy)_2(ClO_4)$, **2**; $Fe_2O(OAc)(tmima)_2(ClO_4)_3$, **3**; (tmima = tris[(1-methylimidazol-2-yl)methyl]amine) and $Fe(ClO_4)_3 \cdot 6H_2O$, **4**, using H_2O_2 as oxidant gave cyclohexanol (CyOH) and cyclohexanone (CyONE). Complex **4** was the most effective and selective, 15-20 turnovers of CyOH, 5-8 turnovers of CyONE, and CyOH/CyONE ratios of ~2. Complexes **1-3** gave 2-7 and 3-8 numbers of turnovers, respectively, with CyOH/CyONE ratios of 0.6-1.1. The presence of an oxidizing intermediate was suggested by iodometric titration in the activation of cyclohexane with complexes **1-4** and H_2O_2. This intermediate was isolated from the reaction mixture and identified by ^{13}C NMR as cyclohexyl hydroperoxide (CyOOH) as compared to an independently prepared sample. The decomposition of CyOOH by **1-4** and H_2O_2 gave CyOH/CyONE ratios of 0.7, 0.9, 0.7, and 2.8, respectively, in the ranges observed in the actual cyclohexane oxidation reactions. These hydrocarbon oxidation reactions were also inhibited by 2,4,6-tri-t-butylphenol. Reactions run under a sweep of argon gave numbers of turnovers 0-31% of the normal values. These results are consistent with a free-radical chain mechanism in which an initially formed cyclohexyl radical is trapped by oxygen to give a cyclohexyl peroxyl radical, which abstracts a hydrogen atom to give CyOOH and carry the chain. Activation of methane, ethane, and propane was also observed.

Biomimetic Oxidation Studies, 6: Synthetic and Mechanistic Aspects of Manganese-Cluster-Catalyzed Alkane Activation Reactions[10]

R.H. Fish, R.H. Fong, K.J. Oberhausen, M.S. Konings, M.C. Vega, G. Christou, J.B. Vincent, and R.M. Buchanan

Manganese clusters $[Mn_2O(O_2CMe)(tmima)_2](ClO_4)_3$ (tmima = tris[(1-methylimidazol-2-yl)methyl]amine), $Mn_3O(O_2CMe)_6(py)_3$, $[Mn_3O(O_2CMe)_6(py)_3](ClO_4)$, $Mn_4O_2(O_2CPh)_7(bipy)_2$, $[Mn_4O_2(O_2CPh)_7(bipy)_2](ClO_4)$, **1-5**, were found to activate ethane, propane, and cyclohexane to their respective alcohols and ketones with monooxygen transfer reagents, t-butyl hydroperoxide (TBHP) or iodosylbenzene (IB), in the presence of O_2. Factors such as solvent, oxidant, catalyst stability, substrate, and presence of O_2 affected the oxidation reactions. Primary kinetic isotope effects (cyclohexane/cyclohexane-d_{12}) were determined to give values of approximately 8 and C-H selectivity studies with adamantane and toluene gave C_3/C_2 values of approximately 10 for the former, while the latter gave a benzaldehyde/benzyl alcohol ratio of 4 with no aromatic ring hydroxylation products, o,m,p-cresols, evident. In addition, the cyclohexane oxidation reactions were studied extensively and found to be quenched when oxygen gas was removed by an argon gas purge, but not effected to any significant extent by the addition of a free radical inhibitor. The overall results imply that a putative Mn=O species is formed, via reaction of Mn catalyst with TBHP or IB, and homolytically abstracts hydrogen from C-H bonds of hydrocarbons to give a carbon radical and Mn-OH. The carbon radical, we speculate, is then trapped by O_2 to form an alkyl peroxy-Mn complex intermediate that rapidly decomposes to alcohol and Mn=O; no alkyl hydroperoxides or alkyl t-butylperoxides were detected. Furthermore, the Mn=O species can abstract hydrogen from the alcohol product to provide the ketone in an O_2 independent reaction.

References

Fish RH, Kim HS, Fong RH. Bonding of mono and polynuclear heteroaromatic nitrogen ligands to (η^5-pentamethylcyclopentadienyl)rhodium dication: structure-reactivity relationships in the formation of nitrogen (η^1) versus $\pi(\eta^5, \eta^6)$ complexes and competition studies of the ligands for the rhodium metal center. *Organometallics* 1991; 10:770.

Fish RH, Kim HS, Fong RH. The bonding mode of nitrogen heterocyclic ligands to (η^5-cyclopentadienyl) ruthenium cation and reactivity studies of the nitrogen and π-bonded complexes: mechanistic aspects of a nitrogen to π rearrangement. *Organometallics* 1991; 10:1965.

Fish RH, Fong RH, Tran A, Baralt E. Heteroaromatic nitrogen ligand studies with (η5-pentamethylcyclopentadienyl) ruthenium cation: η^1, N and $\eta^6(\pi)$ bonding modes and factors that influence a nitrogen to π rearrangement. *Organometallics* 1991; 10:1209.

Fish RH, Baralt E, Smith SJ. Homogeneous catalytic hydrogenation, 5: regioselective hydrogenation of mono- and polynuclear heteroaromatic compounds using the (η^5-pentamethylcyclopentadienyl)rhodium trisacetonitrile dication as the catalyst precursor. *Organometallics* 1991; 10:54.

Fish RH, Konings MS, Oberhausen KJ, Fong RH, Yu WM, Christou G, Vincent JB, Coggin DK, Buchanan RM. Biomimetic oxidation studies, 5: mechanistic aspects of C-H bond activation with Fe, Fe_2O, and Fe_4O_2 complexes in the presence of hydrogen peroxide. *Inorg. Chem.* (in press, 1991).

Fish RH, Fong RH, Oberhausen KJ, Konings MS, Vega MC, Christou G, Vincent JB, Buchanan RM. Biomimetic oxidation studies, 6: synthetic and mechanistic aspects of manganese cluster catalyzed alkane activation reactions. *New J. Chem.* (in press, 1991).

Transport and Physiological Studies of Mammalian Cell Metabolism[8]

H.W. Blanch and D.S. Clark

Protein Production in Mouse Mammary Cells

Our interest in studying mammary epithelial cells from an engineering perspective stems from the observation that unlike most cells in the body, mammary cells are "turned off" most of the time. Only during pregnancy and lactation do these cells become terminally differentiated for milk production. Control of differentiation can be achieved in culture with specific hormonal signals. Because differentiation is readily controlled with these cells and because they can excrete large quantities of proteins (1 gm/10[9] cells/day) they are potentially interesting hosts for genetically engineered protein expression.

We are working with a mouse mammary cell-line (COMMA-1D) isolated from mid-pregnant mice. These cells have been found to secrete caseins (indicative of functional differentiation) in the presence of bovine insulin, hydrocortisone and ovine prolactin (differentiation hormones). A small amount of fetal bovine serum (FBS, 1% by volume), epidermal growth factor (EGF), and bovine insulin (growth hormones) are used to induce cell growth.

In experiments with cells grown on polycarbonate membranes in batch culture, we have been able to induce differentiation by changing the hormonal composition of the medium. Cells were grown on porous polycarbonate membranes (which allow metabolites to enter the cells from the side attached to the membrane, the basal side) batchwise in culture dishes. In growth-hormone containing medium the cells grew to confluence on the membranes, during which time no caseins were made. Upon incubation with differentiation hormones, casein production began and was sustained for 18 days. Casein secretion remained high throughout this 18 day period.

While glucose was rapidly consumed by both growing and differentiated cells, lactate production was markedly different in the two states. Cells in basal medium showed significantly less glucose consumption and lactate production than cells in growth or differentiation medium. Cells in growth medium showed the highest levels of glucose uptake and converted virtually all the glucose consumed to lactate. Cells in differentiation medium showed significantly lower lactate yields than cells in growth medium, particularly cells in which only the basal side medium was changed daily.

Hybridoma Cell Metabolism Studies

Our hybridoma studies have been conducted with an NS1-derived mouse hybridoma cell line (X-D) donated by XOMA. This cell line has been adapted to serum-free medium. As a first step in the overall characterization of the metabolism of this model cell line we have conducted chemostat culture studies. We have measured the steady-state metabolic parameters for the X-D cell line in continuous suspension culture over a wide range of dilution rates. Long term adaptation occurred over the time in culture and resulted in lower glucose consumption rates, reduced lactate production, and higher cell viability. Antibody production rates decreased over the first two months and then remained stable for at least 75 days, even while the culture was subjected to very high dilution rates. The antibody production rate was found to be non-growth associated. Steady-state amino acid production and consumption rates were also determined for a wide range of growth rates. Glutamine, arginine, leucine, isoleucine, and valine (in order of decreasing consumption rate) were consumed at the highest rates. Alanine was produced in large amounts, which is typical for most hybridomas. Alanine is a common sink for glutamine derived ammonia in many mammalian cell types.

We are also conducting ongoing studies of the X-D cell-line in hollow fiber bioreactors which are monitored with the non-invasive technique of NMR spectroscopy. This technique allows us to monitor intracellular metabolite concentrations otherwise not readily measurable. Using the data collected in continuous culture and NMR experiments, we are developing a mechanistic model of hybridoma metabolism. The model is highly structured and includes major regulatory processes of key enzymes involved in primary metabolism. For example, glycolysis is assumed to be controlled by three key enzymes: hexokinase, phosphofructokinase, and pyruvate kinase. The rate expressions for these enzymes include the concentrations of primary regulatory compounds. The resulting system of expressions can be solved numerically, which will allow the prediction of metabolic rates under a wide variety of environmental conditions. Approximations are used for kinetic parameters that can not be measured directly. Results predicted by a preliminary version of this model have been compared to chemostat measurements made for a hybridoma cell-line in our laboratory. The model is able to accurately predict some of the observed experimental results.

References

Fernandez EJ, Clark DS. Magnetic resonance methods in noninvasive studies of bioreactors. (CHEMTECH, in press, 1991)

Hiller GW, Aeschlimann AD, Clark DS, Blanch HW. A kinetic analysis of hybridoma growth and metabolism in continuous suspension culture on serum-free medium. (*Biotechnol. Bioeng.*, in press, 1990)

Sharfstein ST, Gaillard BA, Blanch HW, Clark DS. (accepted for publication by *J. Cell. Physiol.*, 1990)

Separations by Reversible Chemical Complexation[3]

C.J. King, L.J. Poole, L.A. Randel, J.A. Starr, L.A. Tung and V. Van Brunt

Carboxylic acids, glycols and related substances can be manufactured from biomass by fermentation. The economics of such processes are often dominated by the costs of recovering and purifying the desired product from dilute and complex aqueous solutions. The purpose of our research is to investigate reversible chemical complexation with organic complexing agents as a means of economically recovering the desired substances from the aqueous solutions. We have focused on extraction and adsorption, although several other implementations of complexation are feasible as well.

Most of the carboxylic acids with greatest potential for economical production from biomass are relatively non-volatile, e.g., dicarboxylic acids (such as succinic and fumaric acids) and hydroycarboxylic acids (such as citric, lactic, and malic acids). For these substances, regeneration of extractants and adsorbents is challenging because distillation and other methods requiring volatility are not effective. We are currently investigating two novel methods of regeneration that hold strong potential for enhancing the economics of separations by extraction and adsorption.

Regeneration by Precipitation Caused by Selective Dewatering

The first method of regeneration is suitable for extracts of carboxylic acids having low to moderate solubilities. In certain solvents, solubilities of carboxylic acids are substantially increased in the presence of co-dissolved water. This phenomenon enables regeneration of extracts by selective removal of water (e. g., by stripping), accompanied by precipitation of the carboxylic acid. The solubility-enhancement effect attributable to water is particularly pronounced for dicarboxylic acids in ketone solvents, where the increase in solubility is on the order of a factor of eight. We have extensively measured the solubilities of water and three dicarboxylic acids (adipic, succinic, and fumaric) in cyclohexanone and methylcyclohexanone at 25 °C and at 45 °C. These data enable design and evaluation of extraction processes using this method of regeneration. Application has been made for patent protection.

We have also launched efforts to identify other systems for which regeneration by selective removal of co-extracted water would be attractive, and have established that the same phenomenon of enhanced solubility attributable to co-dissolved water occurs for caffeine in ethyl acetate, a common solvent for decaffeination of coffee.

Regeneration by Back-Extraction with Aqueous Trimethylamine

One major complication of fermentation processes for production of many carboxylic acids is that the fermentation operates effectively only at solution pH above the pK_a of the carboxylic acid. (pK_a is the negative logarithm of the first ionization constant of the acid). Under such circumstances the carboxylic acid is largely present as the carboxylate ion. Extraction or adsorption can still be used for recovery of carboxylic acid products from such fermentations if extractants or sorbents with strong enough basicity are used. However, it is difficult to regenerate strongly basic extractants and sorbents.

One effective method for regenerating strongly basic extractants or sorbents is back-extraction or leaching with an aqueous solution of a low-molecular-weight amine, e.g., trimethylamine (TMA). The resultant trialkylammonium carboxylate can be decomposed thermally to yield the product carboxylic acid and the trialkylamine for recycle.

We have determined that near quantitative back-extraction occurs when aqueous TMA is contacted with extracts of lactic, fumaric or succinic acids in a solvent composed of a mixture of Alamine-336 and methyl isobutyl ketone (MiBK). Alamine-336 (Henkel Corp.) is a C_8 to C_{10} tertiary amine and is an effective extractant for carboxylic acids.

We have also shown that succinic acid (pK_a = 4.2) is effectively taken up at high pH by Bio-Rad AG3-X4, a Dowex epoxy-amine resin also containing a small fraction of quaternized ammonium groups. The uptake capacities at pH 5.0, 6.0 and 7.0 are 81%, 65%, and 48%, respectively, of the capacity at pH = 2.7, which is 0.42 g/g sorbent. This sustained capacity is believed to be attributable to sorption of bisuccinate ions onto amine groups and to ion exchange of bisuccinate and/or succinate ions onto quaternized ammonium groups. We have also shown that adsorbed succinic acid can be removed efficiently from Bio-Rad AG3-X4 by leaching with aqueous TMA.

Recovery of Glycols through Boronate Complexation

Boronates complex effectively with many diols, thereby affording a potential means of recovering—and fractionating among—glycols, sugars and related species. Our research has sought to develop an economically attractive recovery method based upon boronate complexation.

Boronates complex only when in the anionic form, and for many boronates ionization occurs only at high pH (e.g., pH 9 and higher). Hence it was desirable to identify a boronate/boronic acid complexant with sufficient acidity to form complexes at lower pH. The nitro group imparts acidity, as does the phenyl group to a lesser extent. We chose 3-nitrophenyl boronic acid (NPBA) as an available boronatewith low water solubility (measured to be 0.40% w/w) and with sufficient acidity to form complexes at pH down to 5.0.

Using the Antikainen titration method, we have measured complexation constants in the aqueous phase as a function of temperature for propylene glycol (1,2-

propanediol) and trimethylene glycol (1,3-propanediol) with NPBA. We are also conducting experiments wherein NPBA is paired with a quaternary ammonium cation in 2-ethylhexanol diluent to form an ion-pair extractant. Measurements of equilibrium distribution ratios for extraction of propylene glycol indicate that recovery of propylene glycol with this solvent is only marginally attractive. However, several other multi-OH solutes of interest (e.g., glycerol, lactic acid, sugars) are known to complex more strongly with boronates, and we are therefore extending our studies to extraction of those substances.

References

Arenson DR, Kertes AS, King CJ. Extraction of ethanol from aqueous solution with phenolic extractants. *Ind. Eng. Chem. Res.* 1990; 29: 607.

Tamada JA, Kertes AS, King CJ. Extraction of carboxylic acids with amine extractants. 1. Equilibria and law-of-mass-action modeling. *Ind. Eng. Chem. Res.* 1990; 29: 1319.

Tamada JA, King CJ. Extraction of carboxylic acids with amine extractants. 2. Chemical interactions and interpretation of data. *Ind. Eng. Chem. Res.* 1990; 29: 1327.

Tamada JA, King CJ. Extraction of carboxylic acids with amine extractants. 3. Effect of temperature, water co-extraction and process considerations. *Ind. Eng. Chem. Res.* 1990; 29: 1333.

King CJ. Separations in the production of high-volume fuels and chemicals by biological processing. In: *Proceedings, Intersociety Energy Conversion Engineering Conference (IECEC)*, Reno NV, August 1990.

Material Applications

Microstructured Materials[10]

A. Hunt, W. Cao, E. Chen, C. Jantzen, and K. Lofftus

Improving the Thermal Performance of Silica Aerogel Superinsulators

The purpose of this research is to substantially enhance the thermal performance of microporous insulating materials. The research involves the preparation, characterization, and heat-transfer analysis of aerogels that are modified to increase their thermal resistance. The thermal resistance of evacuated aerogel is excellent (R-20/inch). However, the resistance can be increased by adding infrared-absorbing and scattering compounds and by introducing structural modifications to reduce the radiative component of heat transfer. In evacuated silica aerogel this radiative component is responsible for up to two-thirds of the thermal conductivity; therefore its reduction by infrared opacification can increase the thermal resistance of silica aerogel by 50% or more. Opacified aerogels should have four or more times the thermal resistance of the best existing CFC-containing polyurethane insulation. Thus, replacing polyurethane insulation with aerogel of the same thickness will provide substantial gains in thermal efficiency in refrigerators and freezers, and will reduce heat losses in piping and energy losses in a variety of industrial applications. Opacifying aerogel also substantially lowers its cost by reducing the amount of raw materials used in its production, thereby increasing the likelihood of its adoption on a commercial scale.

To reduce the infrared heat transfer in partially infrared transparent porous materials, it is necessary to find suitable materials to absorb or scatter infrared radiation in the 3- to 8-micron wavelength region. Several candidates were identified and experiments were carried out to find methods to incorporate these materials into the aerogel. This objective is accomplished by adding either fine particulates or introducing soluble or reacting compounds into the early stages of aerogel preparation. The opacifiers are added after the initial hydrolysis reaction but before gellation takes place. The task is difficult because the opacifiers tend to interfere with gellation or settle out. After gelling and aging, the gels are supercritically dried using the carbon dioxide substitution process developed at LBL. An infrared spectrophotometer is used to evaluate the effectiveness of the opacifier.

Several criteria were developed to identify suitable opacifying agents: they should have a strong absorption or scattering in the appropriate wavelength region to minimize the amount of material required, and form good dispersions in alcosols. Additionally, the agents should not interfere unduly with the sol-gel process and should be non-toxic and low cost. The search for agents was confined largely to inorganic compounds. Various sources of infrared, physical, and chemical data were used to find likely candidates. After the initial selection, experiments were performed to determine dispersion characteristics. Three inorganic candidate materials in the form of solid micro-particles were identified as candidates to absorb or scatter infrared radiation in the 3- to 8-micron region. Two of these materials rely on absorption and one on scattering. They included a transition metal oxide, a carbonate, and an elemental compound.

The experimental work was concentrated in three main areas: 1) development of techniques to improve the dispersion, compatability, and timing of the addition of the infrared opacifiers for the short wavelength band; 2) supercritical drying of coupons for infrared transmission measurements; and 3) development of techniques to prepare larger alcogels for thermal characterization. Methods were explored to produce uniform dispersions of fine particles for infrared opacifiers that can be added to the alcosol prior to gellation. Direct addition at a predetermined viscosity produced dark aerogels but the dispersion was incomplete because of the interaction with the silicon alkoxide. We explored methods of dispersing several types of carbon black into various solutions that settle sufficiently slowly so as to produce a uniformly doped gel. We produced a number of doped alcogel coupons, dried them using the CO_2 substitution process, and measured the infrared spectra of three candidate materials. Infrared measurements showed that the oxide and carbonate opacifiers were unsatisfactory. These materials produced a much lower opacity than predicted using Mie calculations, indicating that a large amount of agglomeration was occurring. Carbon was found to be the best candidate and came closest to its theoretical performance. The infrared measurements demonstrated good potential 3- to 8-micron absorption. The work then concentrated on determining the optimum doping density for the opacifier particles.

Mie scattering programs were developed to predict the absorption and scattering efficiencies of the opacifiers. The literature was searched for methods of heat-transfer analysis in partly transparent media. Several approaches have been developed, all of which are complex. The analysis method that appears most promising is based on the radiation diffusion model. This model will be adapted, and data from the infrared spectroscopy will be used in this model to predict the thermal conductivity for comparison with the experimental results.

References

Lofftus KD, Sastry KVS, Hunt AJ. Colloidal and kinetic principles of sol-gel processing. In: *Advanced Materials Proceedings '90*, 1990.

Lofftus KD. Silica aerogel process modeling and experimental investigations. Ph.D. Dissertation, Materials Science and Mineral Engineering, University of California, Berkeley, 1989.

Light-Scattering Studies[11,12]

A. Hunt, P. Hull, M. Quinby-Hunt, D. Shapiro, C. Gross, R. Macy, F. Orme, A. Quintanilha, and H. Salamon

Light-scattering phenomena involving a variety of microstructured systems were investigated in FY 1990. We have used light scattering from marine micro-organisms to predict the optical properties of the ocean, from red blood cells to explore biomedical processes, from microporous materials to obtain structure information, and from absorbing particles to optimize solar thermal conversion. The light-scattering instrument used for these studies is an angle-scanning, polarization-modulated nephelometer. This nephelometer is capable of completely characterizing elastic light scattering by measuring all 16 elements of the Mueller scattering matrix. Different elements of this matrix can be used to determine specific properties of the scatterers (e.g., shape, optical activity).

Modeling Biological Particles to Predict Optical Properties of the Ocean[11,12]

A. Hunt, P. Hull, M. Quinby-Hunt, and D. Shapiro

Light scattering and visibility in the ocean is being studied through an experimental and analytical program. The scattering by laboratory cultures of micro-organisms is measured and the results are interpreted by comparison with calculations based on analytical models of scattering developed at LBL. The intensity and polarization of scattered light as a function of angle are used to investigate the nature of the particles and to predict the propagation of light in the ocean. The particle population in the ocean is often dominated by organisms with defined size, shape, and optical properties. Thus it is possible to use light scattering to investigate the presence of certain ensembles of organisms in the sea and to predict their effects on the optical properties of the ocean.

In one set of measurements and calculations, four elements of the scattering matrix from Chlorella were compared at 457-nm and 514-nm wavelengths. Chlorella are photosynthetic, single-cell organisms that occur widely, are nearly spherical, and have been called the grass of the sea. The experimental data were corrected for non-spherical contributions. A rigorous calculation of the scattering from a Gaussian distribution of coated spheres (to simulate the internal structure of the cell and size distribution of organisms) was used to model the scattering from Chlorella. Although the absorption of Chlorella have been reported to be strongly wavelength-dependent, the scattering behavior differed only slightly. The sensitivity of the scattering technique

to changes in the imaginary refractive index (absorption), was verified by measuring and calculating the scattering by absorbing and non-absorbing suspensions of well characterized, coated copolymer particles. By fitting four angular-dependent curves simultaneously, we could considerably narrow the range of possible parameters for the particles and determine the index of refraction and thickness of the inner and outer layers of Chlorella.

To explore scattering from non-spherical particles, we studied light scattered by cells of the dinoflagellate *Prorocentrum micans* and irregularly-shaped alumina particles immobilized in a transparent silica gel. One particular matrix element, S_{14} indicates the depolarization of incident circularly-polarized light. The S_{14} signal from the dinoflagellate was found to be significantly larger than that measured for alumina particles of similar size. The nucleus of *P. micans* contains 50-100 structurally complex, chromosomes with a helical structure. The results provided evidence in support of the hypothesis that the observed S_{14} signal produced by *P. micans* is due to the helical nature of the chromosomes.

In related measurements, large circular-polarization signals with strong diurnal variations were observed from solutions of *P. micans*. We are investigating the use of these signals to study aspects of life cycles of dinoflagellates.

Optical Measurements of the Intracellular Polymerization of HbS[11, 12]

A. Hunt, C. Gross, R. Macy, F. Orme, A. Quintanilha, and H. Salamon

We have studied the intracellular polymerization of hemoglobin S in suspensions of sickle cells using circularly polarized light scattering. We have established strong evidence that the preferential scattering of right circular polarized light as measured by S_{14} directly reflects the amount of polymer inside the cells. This technique has made it possible to investigate the effect of oxygen tension, cell density, and osmotic stress on intracellular hemoglobin polymerization. Using the S_{14} signal to determine the amount of hemoglobin polymer, we demonstrated that the polymer increases with deoxyhemoglobin concentration, that cells containing higher hemoglobin concentrations show significantly more polymer than cells containing less hemoglobin, and that polymerization occurs in sickle-trait cells in hypertonic solutions as the oxygen tension in the suspension is reduced. In addition, we were able to measure the kinetics of the polymerization, including that induced by osmotic shock. We also were able to demonstrate that the intensity of the scattered light (that is measured simultaneously with S_{14}) can be used to estimate the percent of reduced (deoxy) Hb in the sample. The work has demonstrated the potential of this technique to monitor hemoglobin polymerization simultaneously with oxygen dissociation under a wide range of physiological conditions.

References

Quinby-Hunt MS, Hunt AJ, Lofftus KD, Shapiro D. Polarized light studies of marine chlorella. *Limnology and Oceanography* 1989; 34:1587.

Hunt AJ, Quinby-Hunt MS, Shapiro DB. Effects of wavelength-dependent absorption on the polarization of light scattered from marine chlorella. In: *Proceedings of Ocean Optics X, SPIE*. 1990; 1302.

Shapiro DB, Quinby-Hunt MS, Hunt AJ. Origin of the induced circular polarization in the light scattered from a dinoflagellate. In: *Proceedings of Ocean Optics X*. SPIE 1990; 1302.

Gross CT, Salamon H, Hunt AJ, Macy RI, Orme F, Quintanilha AT. Hemoglobin polymerization in sickle cells studied by circularly polarized light scattering. (*Journal of Biophysics*, accepted for publication)

Direct Solar-Thermal Conversion Processes

A. Hunt, P. Kuhn, and J. Whitehead

This research explores advanced concepts in the direct conversion of concentrated solar energy to thermal and chemical forms. The energy may be used to drive gas turbine generators, supply industrial process heat, produce useful chemical reactions, or convert solar energy to chemical forms suitable for storage or transport. The current research explores the use of concentrated solar energy in two applications: a high-temperature gas receiver to generate electricity and to initiate chemical reactions. The unifying theme is the absorption of concentrated solar energy by small particles and its conversion to other forms. The concept of using a gas-particle suspension as a solar receiver was first demonstrated by LBL in 1982, and this work laid the foundation for the current research activities.

Solar Photochemical Studies

We are developing a high-temperature gas receiver based on the direct absorption of concentrated sunlight by entrained submicron-sized carbon particles. This effort is part of a multi-year program between investigators in the United States, Germany, Switzerland, and Spain. The goal is to build and solar test a Direct Absorption Particle Injection Receiver (DAPIR) at a major central-receiver solar test facility.

Two forms of entrained-particle receivers have been proposed. The Small Particle Heat Exchange Receiver (SPHER) developed at LBL uses a window to contain a pressurized gas-particle suspension. Bechtel Corporation proposed the Particle Injection Receiver that operates without a window and uses a secondary gas-to-gas heat exchanger. Advantages of both these receivers include high efficiency, high output temperatures, and low cost. In both approaches, the very small mass of carbon particles used to absorb the sunlight is oxidized at the operating temperature to leave a clear gas stream. Therefore, the operating temperature is dependent on the oxidation rate of the particles. In solar testing of the SPHER, it was discovered that the carbon particles oxidized at significantly lower temperatures in concentrated solar flux than when tested under isothermal conditions in the laboratory. This discovery, in addition to making oxidation measurements mandatory, underscores the importance of understanding the general problem of solar flux effects on chemical reaction rates in solid-gas systems.

The objective of the current experiment is to measure the effect of radiant flux on the oxidation rate of carbon particles as a function of temperature. The results will determine the maximum operating temperature for carbon-particle-based gas receivers and provide information to design the DAPIR. The particle oxidation measurements will use the 30 kW solar simulator ("Superbowl") at LBL. It has been equipped with a reaction cell designed and built in Germany. The cell consists of a high-temperature cavity containing a fused silica spiral that carries the dilute gas particle suspension through a region of intense simulated solar radiation. It is designed to maintain the spiral at high temperatures (up to 1000° C), with or without intense solar radiation. The oxidation rate of suspensions of a variety of carbon allotropes will be measured (the thermal oxidation rate of carbon varies by five orders of magnitude depending on the allotrope). The temperature, residence time, and radiant flux will be varied to measure the effects of flux on the particle oxidation rates.

After the carbon oxidation experiment is completed, the equipment will be available for a variety of photo-thermal and photo-chemical experiments. The solar simulator, in combination with the reaction cell and associated equipment, offers a powerful and flexible system for investigating the effects of radiant flux on chemical reactions at high temperatures. In particular, it may be used to study solar detoxification mechanisms and other high-temperature solid-gas reactions for water splitting cycles and chemical processing.

References

Hunt AJ, Hodara I, Miller FJ, Noring JE. Direct absorption receivers for catalyzing chemical reactions. In: Gupta BP and Traugott WH, Eds. *Solar Thermal Technology—Research, Development, and Applications.* 1990; 437.

Kuhn P, Hunt AJ. A new solar simulator to study high temperature solid state reactions with highly concentrated radiation. In: *Proceedings of the 5th Symposium on Solar High Temperature Technologies 1990, Davos, Switzerland.*

Halmann M, Hunt AJ, Spath D. Photodegradation of dichloromethane, tetrachloroethylene, and 1,2-dibromo-3-chloropropane in aqueous suspensions of TiO2 with natural and simulated sunlight. (*Solar Energy Materials*, accepted for publication).

Ultra-sensitive Laser Spectroscopy[9]

R.E. Russo, J.D. Spear, D. Schurig, D. Rojas, P. Robouch†, and R.J. Silva†*

Photoacoustic spectroscopy (PAS) is an ultra-sensitive optical absorption technique for non-destructive chemical analysis. The basis of photoacoustic measurements is the periodic optical absorption in a sample followed by non-radiative conversion of the absorbed energy into heat. A subsequent heat-induced thermal expansion produces a pressure or acoustic pulse in the sample medium whose amplitude is measured by a microphone or piezoelectric transducer. The amplitude of this photoacoustic pulse is directly related to the absorption in the sample, and therefore to the concentration of absorbing species. PAS is a noncontact and non-destructive method capable of determining oxidation states and studying complexation at high sensitivity levels. The sensitivity of PAS surpasses that of conventional absorption spectroscopy by several orders of magnitude.

We developed a photoacoustic spectrometer (Figure) for remote measurements of rare earth and actinide species using an optical fiber to transmit the excitation laser light to a sample solution in a glove box located in a separate laboratory, 85 meters from the laser and detection electronics. The system is ideally suited for conducting actinide research on highly radioactive species in a protected enclosure without requiring sampling and the risk of contaminating the laser laboratory. A pulsed Nd:YAG pumped dye laser (Quanta Ray; DCR 3G/PDL) was used as the excitation light source. The third harmonic of the Nd:YAG (354 nm) was used to pump LD 466 dye (Exciton) with a tuning range from 450-490 nm. This dye was chosen to overlap the absorption bands of Pr^{3+} (praseodymium) at 468 and 482 nm. A 35-mm quartz plano-convex lens (Oriel) was employed to launch the dye-laser light into a fiber. We used an 85-meter multimode optical fiber with a core diameter of 600 µm and cladding diameter of 750 µm (Fiberguide; SPC-600Z). The outer jacket (black Tefzel) increased the total fiber diameter to 1010 µm. The losses in the fiber are specified to be approximately 25 db/km at 500 nm. The fibers' damage threshold is 25 mJ with an 8-ns laser pulse for wavelengths greater than 400 nm. At the remote location, a 10× microscope objective was used to collimate the light from the fiber and direct it into a cuvette containing the sample solution. We did not observe any degradation of the objective with the reduced energy at the distal end of the fiber. The microscope objective was placed 1 cm from the fiber which produced a collimated beam approximately 6 mm in diameter. The photoacoustic cell-assembly consisted of a quartz cuvette acoustically coupled to a cylindrical quartz rod and a piezoelectric transducer. The transducer was PZT (lead-zirconate-titanate) 5A (Vernitron), 0.080 thickness with a 1-MHz resonant frequency. The signal from the PZT was amplified by a charge sensitive preamplifier (Ortec; 142C) and conditioned by a spectroscopy amplifier (Ortec; 570). Gated detection was employed using a boxcar integrator (Stanford Research Systems; SR250). Beer's law linearity was observed over the range of Pr^{3+} concentrations measured. A determination limit of 8×10^{-6} M was a factor of three higher than normally achieved without fibers, primarily because of the lower pulse energy delivered to the sample. A mirror was temporarily used in place of the photodiode/filter assembly to return the laser beam back through the cuvette. This arrangement effectively doubled the power and increased the determination limit by a factor of two; sensitivity is limited by electronic PZT and background absorption fluctuations. In general, the detection capability was exactly that normally achieved in the laboratory without the fiber.

Reference

Russo RE, Rojas D, Robouch P, Silva RJ. Remote photoacoustic measurements in aqueous solutions using an optical fiber. *Rev. Sci. Instrum.* 1990; 61: 3729.

*Visiting scientist (permanent address: Departamento de Quimica, Universidad de Los Andes, Merida 5101, Venezuela).

†Nuclear Chemistry Division, L-396, Lawrence Livermore National Laboraotry, Livermore, CA 94550.

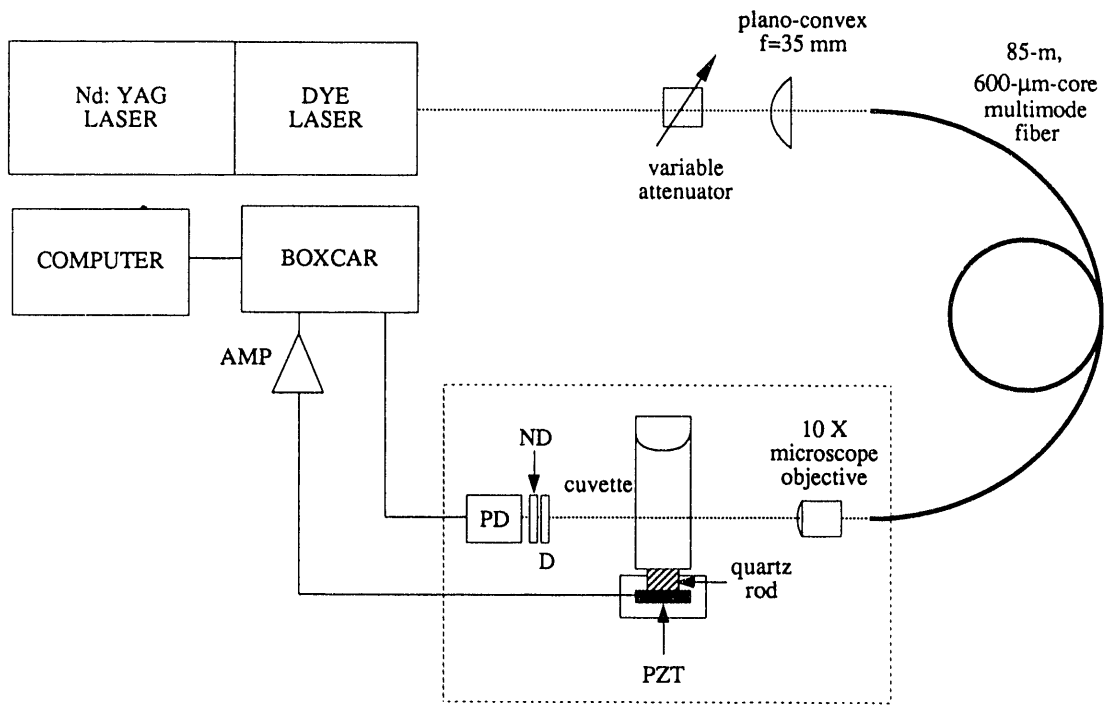

Figure. Diagram for experimental optical-fiber photoacoustic spectrometer.

Electrical Characterization of High-T_c Films[2]

P. Berdahl, J. McMillan, and M. Nicholas

In addition to routine electrical characterization of superconducting films deposited on metal substrates (e.g., resistance and critical current density vs. temperature), we perform novel characterization measurements to further elucidate dissipative mechanisms in high-T_c superconductors.

One particularly interesting measurement has been angular magnetoresistance, in which sample resistance is determined as the sample is slowly rotated in a fixed magnetic field. The high-T_c superconductors are all highly anisotropic, and this anisotropy is directly apparent in the angular magnetoresistance measurements. If the conductor is composed of randomly oriented crystallites, little dependence of resistance on orientation angle is seen. (Demagnetizing effects are nearly absent for fields above about 0.1 tesla, so the shape of the conductor cross section is not very important.) On the other hand, if the crystallites have a dominant orientation (i.e., the conductor has texture), then a pronounced dependence on orientation angle is seen. A minimum in resistance is observed when the magnetic field is aligned parallel to the copper-oxide planes, as may be expected from free energy considerations. For our films, then, c-axis orientation produces a resistance minimum for field parallel to the film, whereas a-axis orientation produces a minimum with field perpendicular to the film. Both types of orientation have been observed in both epitaxial films on crystalline substrates and in films deposited on buffered metal substrates. Angular magnetoresistance measurements generally agree well with, and complement, x-ray diffraction.

References

Russo RE, Reade RP, Berdahl P, McMillan JM, Olsen BL. Fabrication and characterization of YBaCuO thin films on stainless steel substrates. In: *Proceedings of the Second International Symposium on High-Temperature Superconducting Compounds: Processing and Superconducting Properties,* TMS Annual Meeting, Anaheim, CA, 1990.

Berdahl P, Russo R. Progress toward thin-film-based tape conductors. In: *Progress in High-Temperature Superconducting Transistors and Other Devices.* SPIE Conf. Vol. 1394, Santa Clara, CA, 1990.

Sputtering of High-T_c Superconducting Films[2]

M. Rubin, M. Dixon, E. Yin, and B. Hopper

The objective of this task is to develop a practical process for sputtering high-J_c films on polycrystalline substrates. In conventional planar magnetron sputtering, negative oxygen ions are believed to be accelerated towards the substrate, causing deviations from stoichiometry, disorder, and even net resputtering of the film. The most common solution to this problem has been sputtering off-axis at high pressures to slow and avoid the directed beam. This situation is undesirable because of very slow deposition rates and loss of the easily scaleable planar configuration. Biasing of the substrate holder and a secondary electrode on axis at lower pressure greatly increased the deposition rate, but significant damage still occurs from charge-exchanged and reflected neutrals. A combination of biasing and particle shields produced superconducting films on axis.

The above observations about sputtering conditions hold even for a single-crystal substrate like strontium titanate. When a metal tape substrate such as stainless steel or Hastelloy are used, however, superconducting films are never produced unless a buffer layer is introduced. Yttrium-stabilized zirconia and other materials with compatible thermal-expansion coefficients work well as buffers. Auger depth profiling shows that they block diffusion of harmful transition-metal elements from the substrate. There is a strong tendency for the grains to grow with c-axis orientation as revealed by x-ray diffraction, but random nucleation of the grains produces rotational misorientation and weak links. Thus, high T_c's can be obtained, but J_c's fall to typical bulk levels. Future efforts will focus on alignment and recrystallization.

Pulsed Laser Deposition for Thin-Film High-Temperature Superconductors[2]

R.E. Russo, R.P. Reade, X.L. Mao, and E. Faulques†*

Pulsed laser deposition has been employed as an excellent technique for fabricating intermediate layers and high-temperature superconducting (HTSC) thin films on substrates suitable for tape conductors. We have improved the deposition of YBCO and BSCCO thin films on various substrates, with particular emphasis on alloy tapes. These alloys were chosen so that their thermal expansion coefficient bracketed that of YBCO and BSCCO. Progress included developing intermediate layers to protect against interdiffusion, promoting oriented growth of the superconducting film, improving resistive transitions, and increasing critical current density.

Silver was found to act as a good intermediate layer for improving the resistive transition of YBCO films on stainless steel. With a Ag intermediate layer, the as-deposited resistive transition T_c (R = 0) for YBCO was increased to 84 K. Although we were successful in improving T_c for YBCO using Ag intermediate layers, Auger and x-ray diffraction analysis indicated that the Ag was not completely effective in eliminating interdiffusion or providing registry for oriented films, respectively. In addition, the best J_c obtained for these films was only comparable to bulk values.

We deposited intermediate layers of MgO, YSZ (yttria stabilized zirconia), and $SrTiO_3$ on the various alloy substrates. These materials are more refractory at the deposition temperature used for YBCO and BSCCO, and can provide registry for epitaxial growth of the superconducting films. A series of YSZ intermediate layers was deposited on the nickel based stainless steel alloy (thermal expansion coefficient comparable to YBCO and BSCCO). By changing the pressure and temperature, we are able to control the growth of a particular orientation, either the 111 or 001 orientation are dominant under different conditions. Auger measurements were completed on various stainless steel substrates with intermediate layers and YBCO films. Laser deposited YSZ, $SrTiO_3$ and MgO intermediate layers exhibited sharp boundaries at the YBCO and stainless steel interfaces. Excellent as-deposited YBCO films were grown on the 001 oriented YSZ (Figure 1). The T_c was normally 86 K on the 001 YSZ and approximately 82-84 K on the 111 YSZ. J_c was highest for the YBCO films on the 001 YSZ, approximately 4000 A/cm^2 at 77 K. In all cases, the J_c was lower for films on the 111 YSZ (Figure 1). The as-deposited T_c (R = 0) for YBCO using 001 YSZ layers is among the best ever reported.

*Visiting scientist from University of Science and Technology, Hefei, China.
†Visiting scientist from Universite de Nantes, Nantes, France.

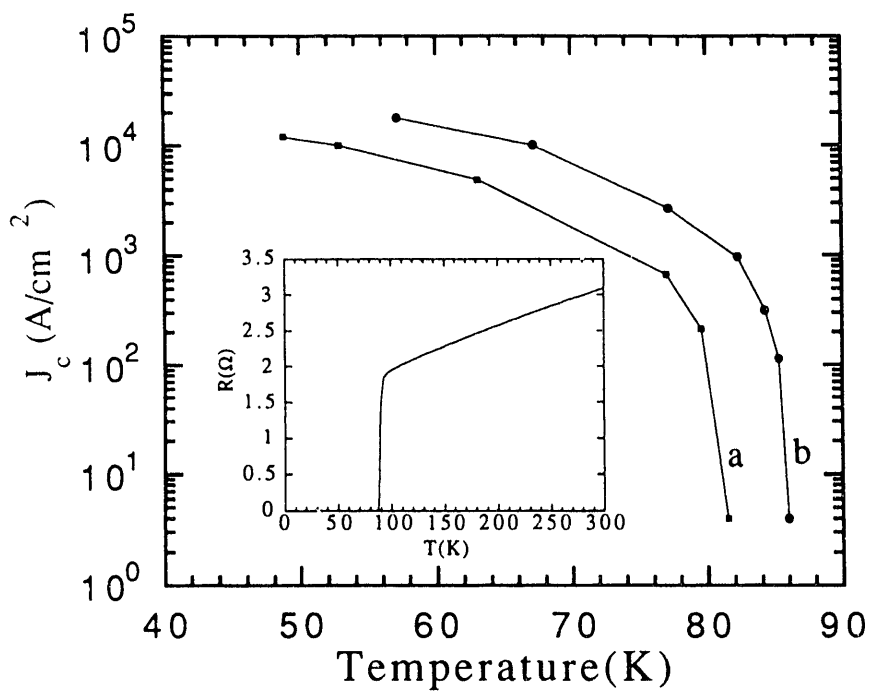

Figure 1. Critical current densities of YBCO films on a) (111) YSZ, and b) (001) YSZ intermediate layers as a function of temperature. Inset shows resistance versus temperature data for the film on (001) YSZ.

We made excellent progress with the deposition of BSCCO thin films on MgO. This work was conducted as necessary preliminary studies to the fabrication of BSCCO on the stainless steel tapes. A series of bulk BSCCO targets were fabricated containing various amounts of Pb and Sb substituted for Bi. For most of the targets, the 2223 phase was stabilized with T_c (R = 0) at 110 K. Using a target with the 2212 phase, we deposited thin films with predominantly 2212 phase and T_c (R = 0) at approximately 72 K, after annealing at 830°C for 10 min. in air. The T_c was equal to that of the bulk material. We then successfully deposited the 2212 phase of BSCCO without post annealing when the target composition included Sb (Figure 2a). In all cases in which 2212 phase was obtained, the substrate temperature was approximately 800°C and pressure 200 mtorr oxygen. As seen in Figure 2a, this as-deposited film exhibits a T_c (R = 0) at approximately 70 K. For several of the films, a slight decrease occurred at 110 K characteristic of the 2223 phase. X-ray diffraction analysis confirmed the existence of primarily 2212 phase with minimal 2223 phase in many of the BSCCO films on MgO (Figure 2b). Our BSCCO thin film results are very encouraging, only two other laboratories in the world have achieved similar transitions for as-deposited BSCCO films. We fabricated the first as-deposited BSCCO thin-film on stainless steel with a resistance transition to zero; the zero resistance temperature was approximately 22 K. The target contained 0.1 Sb and 0.3 Pb. X-ray diffraction analysis of this film showed 2201, 2212, and 2223 phases. The laser deposited intermediate layer was $SrTiO_3$. These results were confirmed by a second as-deposited BSCCO thin film on stainless steel with a resistance transition at 24 K.

References

Russo RE, Reade RP, McMillan JM, Olsen BL. Metal buffer layers and YBaCuO thin films on Pt and stainless steel using pulsed laser deposition. *J. Appl. Phys.* 1990; 68:1354.

Reade RP, Mao XL, Russo RE. Characterization of YBaCuO thin films and yttria stabilized zirconia intermediate layers on metal alloys by pulsed laser deposition. *Applied Physics Letters* 1991; 59:739.

Mao XL, Russo RE, Liu HB, Ho JC. As-deposited Sb doped BiPbSrCaCuO thin films prepared by pulsed laser deposition. *Applied Physics Letters* 1990; 57:2591.

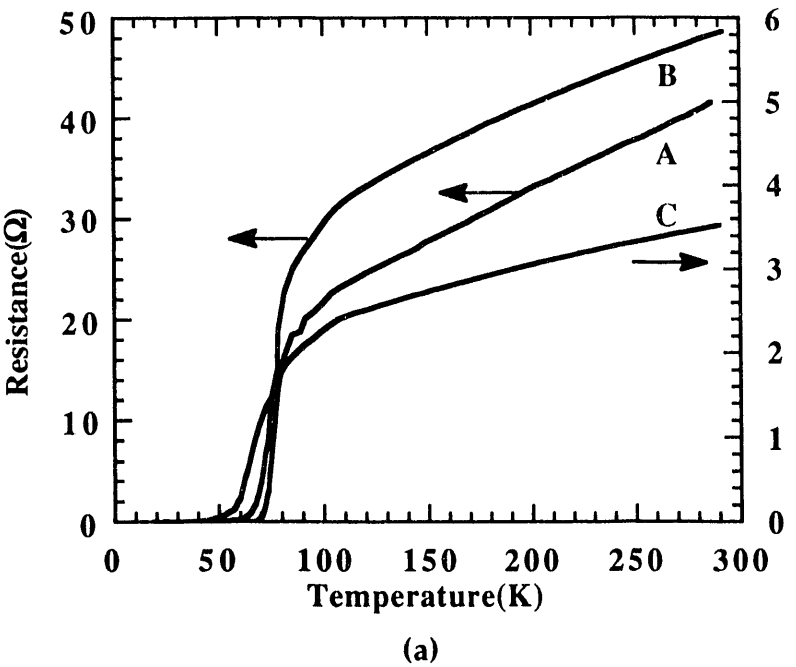

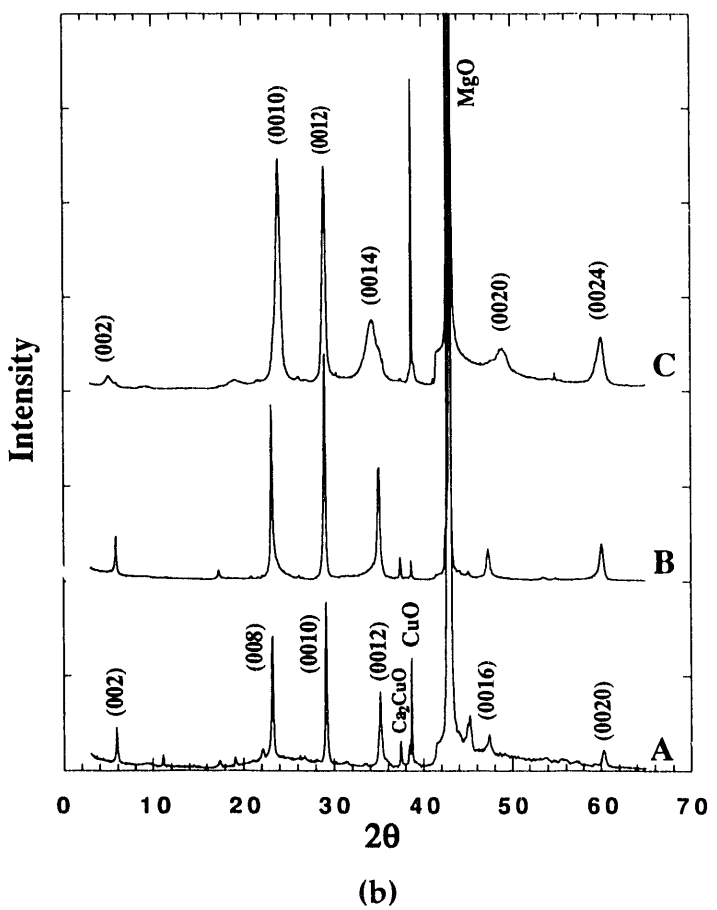

Figures 2a-b.
The (a) resistance versus temperature -dependence and (b) x-ray diffraction for as-deposited BSCCO films on MgO. A and B are films deposited from an Sb-doped target; film C is deposited from a target without Sb.

Repetitively Pulsed Laser Material Interactions and Steady-State Laser Sampling[10]

*R.E. Russo, W.-T. Chan, M.A. Shannon, D. Schurig, and A.A. Rostami**

This research involves study of the mechanisms which influence the explosive removal of solid material by high power pulsed laser radiation and the use of a repetitively pulsed laser material interaction for steady state sampling in chemical analysis. Under suitable conditions, a repetitively pulsed laser can provide continuous sampling and steady state atomic emission intensity from an analytical excitation source. Compared to a single-pulse interaction, the steady state response provides better reproducibility for analysis, and a more-controlled environment for studying the laser-material interaction. We have initiated studies involving atomic emission spectroscopy, acoustic monitoring, and optical probe beam deflection for studying the repetitively pulsed laser material interaction.

Atomic Emission Spectroscopy

A cylindrical chamber with a water cooled mount was constructed to accommodate disc-shaped solid samples. A KrF excimer laser (λ= 248 nm) beam was focused on the solid samples to initiate an ablation interaction. The ablated material was transported to an inductively coupled plasma (ICP) from which elemental emission intensity was monitored using a monochromator with a photodiode array (PDA). The ICP serves as the excitation source for atomic emission spectroscopy (AES) and as a real-time monitor of the laser material interaction. The ICP is an excellent excitation source because of its high temperature and ability to dissociate stable molecules or cluster that can form during the laser pulse. The PDA controller enables flexible configuration of the pixels (e.g., grouping and skipping certain pixels), as well as fast analog-digital conversion (ADC) and rapid data transfer to a host computer through direct memory access (DMA). The PDA can be freely rotated. In the horizontal position, the PDA measures a spectral range of 40 or 60 nm, depending on the grating used. In the vertical position, the PDA measures the vertical emission profile in the ICP at a selected wavelength.

Simultaneous elemental emission intensity and temporal profiles were studied from single-pulsed and repetitive-pulsed laser solid interactions. Preliminary studies involved monitoring copper atomic emission intensity in the ICP resulting from laser sampling on pure copper, brass, and bronze discs. Figure 1 shows the capability of the PDA by showing its response to a single laser pulse interaction on a brass target. The temporal study of the emission signal shows that ablated material from a single laser pulse arrives at the ICP discharge with fast rising edge and an exponential decay that lasts several seconds. For repetitive pulsing, PDA profiles showed the first few laser pulses generated more ablated material than successive pulses, but a steady state signal intensity for individual elements could be obtained. Steady state signal intensity from the ablation of copper increased with fluence (constant energy) from 0.3 to 0.8 GW/cm^2, and then leveled off at 0.8 to about 3 GW/cm^2 (Figure 2). Using ICP-AES, we have also demonstrated the ability to detect particles generated during the interaction, an induced pressure pulse, and the ratio of elements from alloy targets. The elemental ratio was found to be a function of the incident power density.

Acoustic Monitoring

Piezoelectrics (attached directly to the solid) were used to study the propagation of acoustic waves induced in the material by pulsed laser irradiation, in order to indicate the existence and time dependence for mechanisms of heating, melting, vaporization, and ablation. A sensor was developed for monitoring the amplitude and frequency response of the acoustic wave induced in the solid material. Frequency bandwidth of the piezoelectric transducer (PZT) and acoustic reflections were determined to be the primary factors that influenced the measured response. Based on the use of a 8-nsec laser pulse, the acoustic pulse has its maximum frequency at approximately 20 MHz, and contained much lower, even audible frequencies. To obtain this frequency bandwidth requires thin PZTs (0.25 mm) or thin-film polymeric materials. In addition, the reflection coefficient at all interfaces must be less than 0.1; therefore, the materials must be chosen with the same acoustic impedance. The initial identified materials were copper, brass, acrylic, and lead-zirconate-titanate piezoelectrics. A cylinder rod assembly employing a copper sample, PZT, and acrylic backing plate was constructed to monitor the laser material interaction. Initial results were compared to a finite difference model of the system.

Optical Probe Beam Deflection

Optical probe beam deflection (OPBD) was employed to

* Visiting scientist (permanent address: Mechanical Engineering Department, Isfahan University of Technology, Isfahan, Iran).

monitor the region adjacent to the solid surface, in order to determine heating and cooling rates, the onset of material removal, and the formation of a laser initiated surface plasma. A modulated cw Nd:YAG laser was employed as the heating source. The deflection of a HeNe laser beam propagating in air adjacent to the heated solid surface was measured with a linear position sensor. The deflection amplitude increased linearly with laser power until melting occurred, at which time the response became erratic. Several factors were identified to influence the OPBD signal. Primarily, changes in the local geometry during a phase change have a profound effect on the heat transfer into the solid material. Therefore, the temperature gradient in the adjacent medium will be influenced by local geometry changes in the heated solid target. Geometric effects on the OPBD signal were investigated using finite-difference analysis and compared with experimental results using Cu and Pb targets. Initial experiments were conducted in the linear heating regime (without phase change) in order to unambiguously study the effect of boundary conditions and thermal diffusivity on the OPBD signal. Shallow craters with different aspect ratios were drilled into the sample surface. The crater diameters were less than, equal to, and greater than the excitation beam diameter (approximately 0.5 mm). The results indicated significant differences in the probe beam response shape and amplitude as a function of crater geometry. Experimental measurements showed that the OPBD signal magnitude and phase differed by up to 70% from those measured from flat-plane geometries when the radius of spherical craters was approximately equal to that of the heating laser beam. Vaporization, melt ejection, and ablation will cause transient and permanent changes in the local geometry that influence the OPBD signal at least as severe as for the static geometry case.

References

Chan WT, Russo RE. Study of laser material interactions using inductively coupled plasma atomic emission spectroscopy. *Spectrochim. Acta, Part B* 1991; 46:1471.

Shannon MA, Rostami AA, Russo RE. Photothermal deflection measurements for monitoring heat-transfer during modulated laser heating of solids. *J. Appl. Phys.* 1992; 71:53.

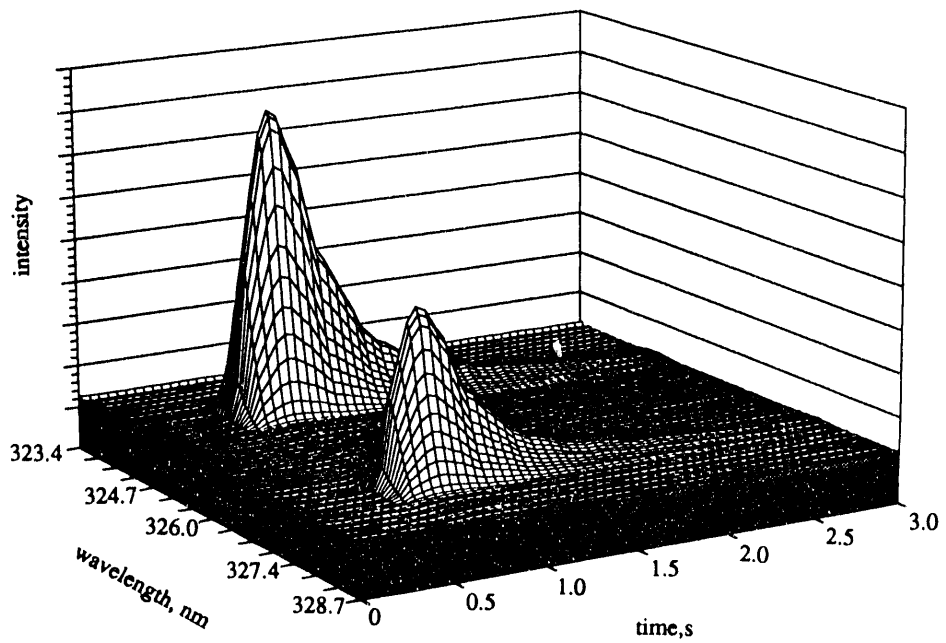

Figure 1.
Photodiode array response from Cu emission in the ICP resulting from single-pulse laser sampling.

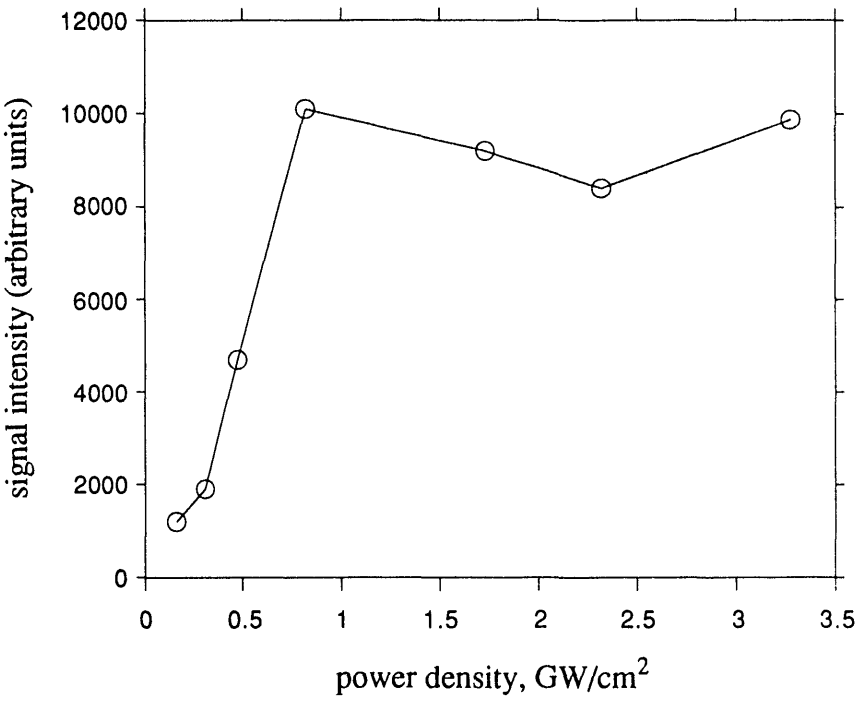

Figure 2.
Steady-state Cu emission intensity versus laser fluence during repetitive laser sampling.

Projects described in this report were supported by the following sources (funding sources for individual projects are keyed to this list; see superscipt numbers following project titles):

Assistant Secretary for Conservation and Renewable Energy:

1 Deputy Assistant Secretary for Utility Technologies, Office of Energy Management , Advanced Utility Concepts Division

2 Deputy Assistant Secretary for Utility Technologies, Office of Energy Management , Advanced Utility Concepts Division, Superconducting Technology for Electric Power and Systems (STEPS)

3 Office of Energy Systems Research, Energy Conversion and Utilization Technologies (ECUT) Division

4 Office of Industrial Technologies, Advanced Industrial Materials Program (AIM)

5 Office of Transportation Technologies, Electric and Hybrid Propulsion Division

6 Defense Advanced Research Projects Agency (DoD), Advanced Vehicle Systems Technology Office, for Naval Sea Systems Command (NAVSEA) under MIPR #N0002490MP70004, ARPA Order #6413:22

7 Morgantown Energy Technology Center, Assistant Secretary for Fossil Energy, Office of Coal Utilization, Advanced Research and Technology Development, Division of Surface Coal Gasification

8 University of California Systemwide Biotechnology Research and Education Program

9 Lawrence Livermore National Laboratory Contract No. W-7405-ENG-48

10 Director, Office of Energy Research, Office of Basic Energy Sciences, Chemical Sciences Division

11 National Institutes of Health through the National Heart, Lung and Blood Institute

12 Environmental Sciences Program, Directorate of the Office of Naval Research

13 Electric Power Research Institute (EPRI)

This support was provided through the U.S. Department of Energy under Contract No. DE-AC03-76SF00098.

END

DATE FILMED

11/10/92